



Geological Survey Ireland
Tellus A5 Block: *aempy*
Electromagnetic Inversion Report

*Geological Survey Ireland is a division of the Department
of Communications, Climate Action & Environment.*



Geological Survey
Suirbhéireacht Gheolaíochta
Ireland | Éireann

Document Information

Project title:
Tellus A5 Block: aempy Electromagnetic Inversion Report
Current Document version 1.4 Date 25/02/2020

Prepared By	Date	Comment
M. R. Muller	25/02/2020	Responses to V1.3 implemented in V1.4

Reviewed By	Date	Comment
Jim Hodgson	18/02/2020	Review of V1.3

Approved By	Date	Comment
Insert name	00/00/0000	

Version History

Ver. No.	Ver. Date	Comment	Revised By
1.0	15/02/2020		M. R. Muller
1.3	18/02/2020		J. A. Hodgson
1.4	25/02/2020		M. R. Muller



Table of Contents

Table of Contents.....	ii
1. Introduction.....	1
Background to Tellus.....	1
Background and Rationale for Inversion Modelling	1
Inversion Approach and Strategy.....	3
Summary of Inversion Products Delivered	6
2. <i>aempy</i> Toolbox	7
Overview of Toolbox Utilities.....	7
Tikhonov-type Regularised 1-D Layered Inversion	8
Principal Component Analysis Filter	10
3. Inversion Parameter Testing.....	12
Laser Altimeter (Clearance) Smoothing	17
Principal Component Analysis Noise-Rejection Filter	19
Independent versus Non-independent Inversion.....	23
Averaging of Non-independent Inversion Models (FRA Strategy).....	26
Inversion Regularisation Parameters.....	28
EM Component Data Errors	34
4. Data Inversion	43
Inversion Parameters	43
Evaluation of Models and Fit	45
5. Model Cleaning.....	55
QC Parameter Threshold Rejection	57



Smoothing, Outlier Resistivity Value Rejection63

Microlevelling of Resistivity Model Data64

Model Data Released70

6. Conclusions.....72

7. References.....74

Appendix 1: A5_EM_INV_MODELS_OHMM_ReadMe.txt.....75

Appendix 2: A5_EM_INV_MODELS_OHMM_GRIDS_ReadMe.txt77



1. Introduction

Background to Tellus

Tellus is a national programme to gather geochemical and geophysical data across the island of Ireland. The survey examines the chemical and physical properties of our soils, rocks and waters to inform the management of Ireland's environment and natural resources. The project is managed by Geological Survey Ireland and is funded by the Department of Communications, Climate Action and Environment (DCCAE).

The Tellus airborne geophysics survey, collecting magnetic, gamma-ray spectrometry and electromagnetic (EM) data, follows on from the initial Tellus Survey of Northern Ireland in 2005-2006, with the first survey carried out in Ireland in 2011. Since then, annual survey blocks have generally progressed southwards through the country. To date, 10 distinct survey blocks have been flown in Ireland with all data processed and made publically available at www.gsi.ie/tellus. Data from the A5 Survey Block, flown over county Limerick in 2018-2019, are used as the first test case for inversion modelling of Tellus EM data.

Background and Rationale for Inversion Modelling

Tellus airborne electromagnetic (EM) data, with the exception of one survey block flown in 2014-2015, are acquired with a four-frequency frequency-domain (FEM) system utilising transmission frequencies at 912, 3,005, 11,962 and 24,510 Hz. Orthogonal in-phase and quadrature components of the EM response at each frequency are recorded and subsequently processed independently of each other, providing eight components of data at each measurement location. The nominal flight speed of 60 m/s and 10 Hz EM data sampling rate provides measurement locations at approximately 6 m interval along the flight lines.

Geologically more useful subsurface electrical resistivity data can be derived from the eight-component EM response data using a range of different modelling strategies. To date, all resistivity products generated and published by the Tellus program have been based on separate and independent modelling of each of the four frequencies, providing independent resistivity data (either as flight-line data or maps) at each frequency (i.e.,



single frequency modelling). The highest frequency resistivity data, at 24,510 Hz, provide the shallowest, near-surface imaging, while the lowest frequency data, at 912 Hz, provide the deepest subsurface imaging, to depths in the range 40 – 100 m, depending on the subsurface resistivity itself. Greater depths of EM penetration are achieved where the subsurface rock materials are more resistive (i.e., less conductive).

The merged EM resistivity maps (consisting of all contiguous data blocks to date) currently published by the Tellus programme for each EM frequency are derived by Geological Survey Ireland using the *Geosoft HEM* software module. In the *HEM* inversion scheme a single half-space resistivity value is determined, through formal inversion, that best matches the input in-phase and quadrature data at each measurement location, separately for each of the four EM frequencies.

Published resistivity data for each of the separate, completed survey blocks are produced by contractor Sander Geophysics Limited (SGL) using a nomogram (look-up table) approach. In this approach, the resistivity models are generated using the combination of two nomogram-based resistivity algorithms: (i) a pseudo-layer resistivity for areas of strong signal and (ii) an amplitude-altitude algorithm for areas of low signal (i.e., high resistivity areas). The nomograms identify a matching half-space resistivity value for in-phase and quadrature data pairs at each measurement location and for each frequency independently.

SGL subsequently use EM skin-depth as a means of estimating approximately the subsurface imaging depth corresponding with each resistivity data point at each frequency. In the skin-depth equation, depth of EM signal penetration (δ , in m) (to 1/e of the original signal amplitude) is dependent on the signal frequency (f , in Hz) and the ground resistivity (ρ , in $\Omega.m$):

$$\delta = 503(\rho/f)^{1/2} \quad (1)$$

SGL define the depth of imaging (or centroid depth) as $\delta/2$ and, through a process of lateral and vertical interpolation of depth-resistivity pairs derived from each of the four frequencies, produce resistivity-depth data and map slices at 10 m, 30 m, 60 m and 100 m depths. More information on SGL's depth estimation approach may be found in SGL's A5 Block Technical Report (SGL, 2019), and in Sengpiel (1988) and Sengpiel and Siemon (1998).



While these approximate resistivity-depth products have proven excellent for the mapping of lateral geological variation, they lack the depth resolution and accuracy needed for reliably understanding the geological variation with depth and, for example, for constructing vertical geological cross-sections. GSI has responded to data-users' needs for better depth constraints in the resistivity products offered by Tellus by carrying out formal 1D inversion of the EM response data, modelling all eight EM data components simultaneously at each measurement site. Inversion of the EM data was done using the *aempy* suite of software tools, a new open source, *Python* based EM processing and modelling "toolbox" developed by researchers at Dublin Institute for Advanced Studies, funded by a GSI Short Call Research Award (Kiyani and Rath, 2017; Kiyani *et al.*, in review). The reasons for electing to use the *aempy* toolbox and for the inversion approach developed around its capacities are discussed further below.

The release of EM inversion resistivity models for the Tellus A5 Block is the first such data release by the Tellus programme, and the methodology used in the inversions is therefore presented in some detail in this report. Modelling of all previously flown data blocks is ongoing and EM inversion models for these blocks will be released as completed.

Inversion Approach and Strategy

The need to process and invert large volumes of EM data places a number of requirements on the inversion strategy used and on the inversion codes that support it.

The primary requirements are:

- i. Automation of the process as far as possible.
- ii. Generation of a range of inversion-model quality-control (QC) parameters that can be used collectively for automated, objective rejection of poor model solutions. The recorded EM data are subject to high cultural noise levels across many parts of Ireland and geological signal strength is strongly attenuated in high-fly zones, both of which impact on the reliability and quality of the EM inversion models.
- iii. Relatively fast inversion computational speeds.



Three different commercial and non-commercial codes were tested and assessed by GSI: *EMIGMA* (Petroseikon), *EM1DFM* (University of British Columbia) and *aempy*. All three codes implement similar Tikhonov-type, smooth, regularised 1-D EM inversion schemes and produce similar and comparable output resistivity models. While the *EM1DFM* and *aempy* codes were found to be similar in computation speed, that of *EMIGMA* is somewhat slower. One of the main advantages of the *aempy* toolbox lies in its *Python* coding, allowing the development of customised scripts for automation and for customised output of inversion models and desired model quality-control parameters. The capacities of the *aempy* toolbox, which include both inversion and pre-inversion processing and filtering tools, are discussed in detail further below.

The inversion workflow is summarised in Figure 1.1 and consists of three main components, implemented as indicated using the facilities of both *aempy* and *Geosoft Oasis Montaj* software: (i) EM and altimeter data pre-processing and filtering, (ii) automated 1-D EM inversion on a line-by-line basis and computation and output of resistivity models and quality-control parameters and (iii) model cleaning (rejection of unreliable model solutions) using quality-control parameters, line-to-line microleveling and model output. Details of each component of the workflow are discussed in sections of the report that follow below, as well as details of the comprehensive tests undertaken to define the optimum control parameters for each workflow component.

The emphasis in the testing and choice of parameters for the inversions and model cleaning process was to identify and use parameters most appropriate for the A5 dataset as a whole – to avoid the inclusion of artefacts and unreliable model solutions in the final delivered model data. It may be the case, therefore, that some resolution and detail is lost in local areas, and which could potentially be recovered using inversion and model cleaning parameters and strategies optimised specifically for those areas. To support Tellus end-users in exploring the possibility of deriving higher resolution EM resistivity models in local areas of interest, the *aempy* software and scripts are made freely available and may be obtained by email enquiry to tellus@gsi.ie.



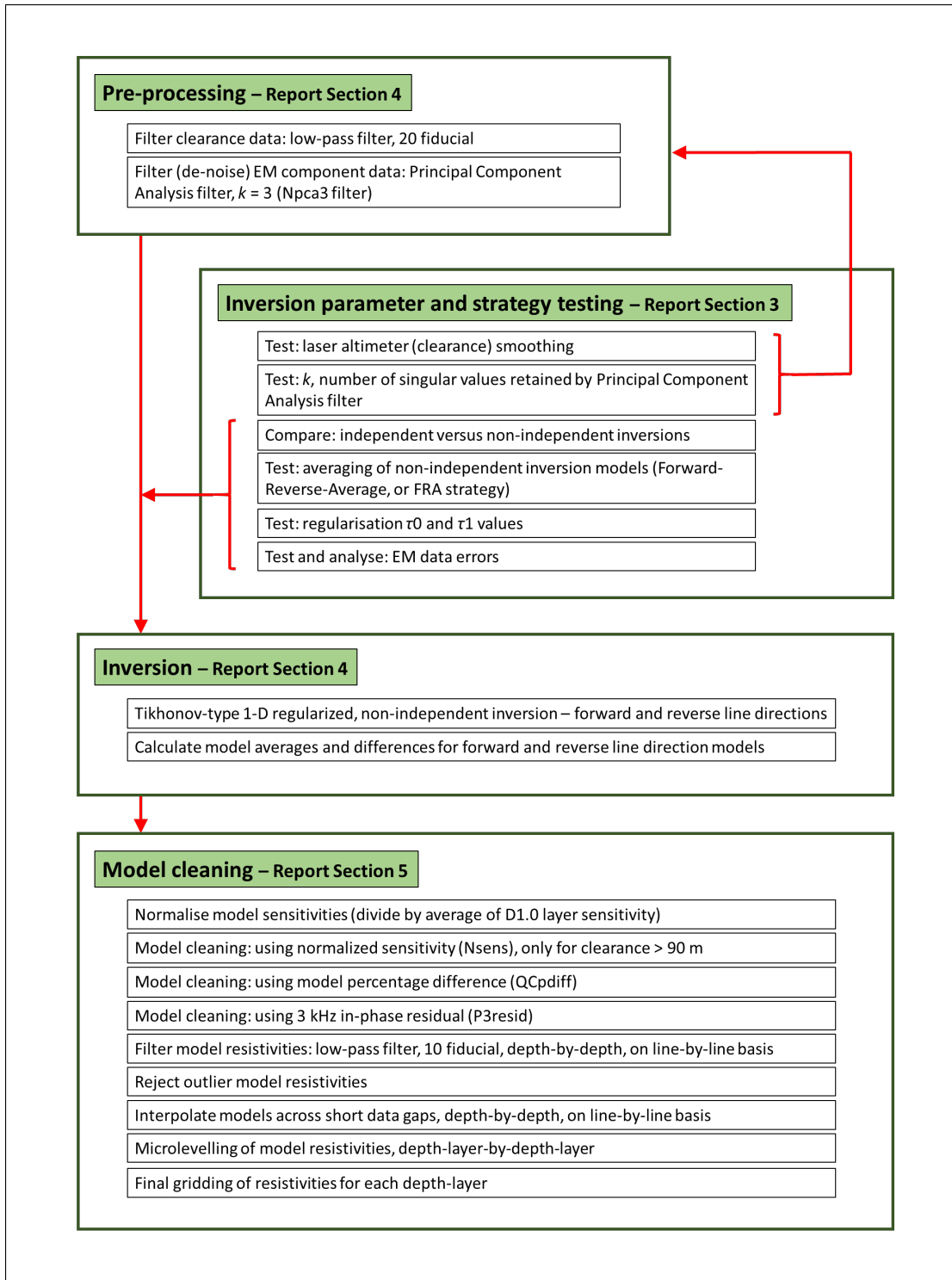


Figure 1.1: Schematic illustration of the EM inversion workflow. Each component of the workflow is discussed further in the text below, in Report Sections referred to in the figure.



Summary of Inversion Products Delivered

EM inversion resistivity models, to a depth of 62.6 m, are made publically available, at www.gsi.ie/tellus, in a number of different data formats.

- i. **Ascii, flight-line and site ordered dataset.** Complete, full-resolution dataset with nominal 6 m spacing between model sites. Resistivity data for twenty depth-layers, from 1.0 m to 62.6 m depth, are provided as separate channels (columns) in the dataset. The data are suitable for manipulation to produce either section or map views of the models. Surface topography (DEM) with respect to sea-level is included for each site, allowing models to be plotted beneath a topographic reference in section view.

File name: [A5_EM_INV_MODELS_OHMM.XYZ].

File format: *Geosoft* [.XYZ]. Suitable for import into to any software with an ascii import capability.

Dataset description: Appendix 1.

- ii. **Resistivity grids on 50 x 50 m mesh.** Provided separately for twenty depth-layers, from 1.0 m to 62.6 m depth.

File formats: *Geosoft* grid [.GRD] and georeferenced tiff [.TIF]

Dataset description: Appendix 2.



2. *aempy* Toolbox

Overview of Toolbox Utilities

The *aempy* Toolbox (Kiyani and Rath, 2017; Kiyani *et al.*, in review) is a flexible package of software providing capacity for the 1-D inversion of frequency- and time-domain airborne EM (AEM) data. The software is written in the *Python* language and calls on several numerical packages in *Python*, namely *numpy*, *scipy* and *matplotlib*. Capacities of the toolbox are implemented in a number of high-level scripts that cover a full work flow from (i) loading and reformatting of raw EM data, (ii) pre-processing of EM responses, (iii) inversion modelling and (iv) visualisation of outputs.

- i. Data management tools include reformatting of raw EM data to an internal *aempy* format, data subset selection based on polygons or rectangles, projection of data onto a new profile, and various graphical visualisations of the input data.
- ii. EM data pre-processing functions include the masking of non-physical data, interpolation, and Principal Component Analysis (PCA) filtering of data for noise rejection. (In the case of the A5 Block inversion, only PCA filtering was utilised, with no data masking or interpolation applied).
- iii. Implementation of several 1-D EM inversion approaches:
 - Tikhonov-type regularised inversion. (Used for A5 Block inversion)
 - Bayesian MAP (maximum *a posteriori* probability) inversion in parameter and data space. (Not used for A5 Block inversion)
 - Full Bayesian Markov Chain Monte Carlo (MCMC) inversion. (Not used for A5 Block inversion).
- iv. Various graphical visualisations of: input and filtered EM responses, observed and predicted EM responses (post-inversion), and resistivity model cross-sections.



Tikhonov-type Regularised 1-D Layered Inversion

The computational core of the Tikhonov-type 1-D layered inversion is based on an adapted forward modeller taken from the well-tested **AirBeo** open-source (*Fortran 90*) code. This code was originally developed by Australia's CSIRO and the AMIRA consortium (the latest version of which is available from <https://sourceforge.net/projects/p223suite>). The inversion code in *aempy* is customised for the physical configuration of the current Tellus airborne EM system: the AEM-05 system, which operates at four frequencies (912 Hz, 3,005 Hz, 11,962 Hz, and 24,510 Hz), with vertical, co-planar transmitter and receiver coils (VCP or CpX configuration) mounted at the tips of the aircraft wings with fixed coil separations of 21.35 m for 912 and 3,005 Hz and 21.38 m for 11,962 and 24,510 Hz.

Up to seven geophysical parameters can be included in the 1-D models for inversion: layer thickness, electrical resistivity, relative dielectric constant (although negligible for Tellus EM frequencies), relative magnetic permeability and three Cole-Cole induced polarisation (IP) parameters (chargeability, time constant and frequency constant). The capacity to invert for parameters other than electrical resistivity provides interesting potential when modelling EM data acquired over highly magnetic or polarisable (e.g., clay and disseminated sulphide) lithologies. Practically, however, and subject to future testing, it may be difficult to derive reliably such a large number of rock parameters from the four-frequency Tellus data. The A5 Block EM data were inverted for a single parameter only, resistivity, using fixed layer thicknesses and depths for all sites (defined in Table 4.2, Section 4). The single-parameter, fixed layer inversions should, in principle, provide the best possible resolution in estimating resistivity values.

On the data input side of the inversion, any of the individual eight EM data components can be flagged as active or inactive for the inversion (all eight components were flagged active for the A5 Block inversion) and data errors for the eight components can be individually specified. EM measurement sites can be excluded from the inversion using flight clearance and power-line monitor thresholds (neither threshold was applied to exclude data for the A5 Block inversion).

The theoretical and numerical basis for the Tikhonov-type inversion scheme implemented in *aempy* is outlined in detail Kiyani and Rath (2017) and Kiyani *et al.* (in



review). From a practical user's perspective, there are three parameters requiring definition that control the inversion and the characteristics of the output models: the data errors, and the two regularisation parameters, τ_0 and τ_1 . The parameter τ_0 controls the freedom of the inversion model to diverge from the defined starting (*a priori*) model, with larger τ_0 values providing less freedom. The parameter τ_1 controls the smoothness of the model (in a 1-D vertical sense), with larger τ_1 values producing smoother models. Assignment of a data error to each of the EM data components controls the weighting placed on those components in the inversion. Lower errors provide a stronger weighting. Data errors therefore have the practical effect of focussing the inversion on different regions of the subsurface: for example, lower errors assigned to higher frequency data will tend to weight the inversion towards resolving shallower resistivity structure, and *vice versa* for lower errors assigned to lower frequency data and deeper structure. Given the importance of these three parameters in controlling the inversion outputs, it is beneficial to carry out tests on the inversion dataset, to identify appropriate values for them and to understand how their variation affects the shape and quality of fit of the output models (such tests were carried out for the A5 Block data, as reported in Section 3).

A valuable, post-inversion output provided by the *aempy* code is the model sensitivity matrix (essentially the inversion Jacobian matrix). It describes the sensitivity of the EM responses to changes in the model resistivity, separately for each layer at depth in the model. Numerically, sensitivity, S , is defined as the derivative of the EM response, $g(m)$, with respect to the model parameter, m (resistivity):

$$S = \partial g(m) / \partial m \quad (2)$$

where the net sensitivity is provided by the sum of the sensitivities of all eight data responses (components). Where a large change in model resistivity (for a particular depth layer) produces a small change in the predicted EM response, that part of the model might be regarded as poorly constrained, as the EM data are insensitive to it. As the Jacobian matrix in the inversion is weighted by the data errors, higher data errors lead to lower model sensitivities. Sensitivities are intimately connected to the specifics of the EM data acquisition system and the inversion parameterisation: e.g., the frequencies used and the coil geometry, the flight clearance, the data errors assigned, and the thickness of the model layers (thinner layers have lower sensitivities). It is



therefore very difficult to assign a universal sensitivity threshold above which a model solution might be regarded as reliable. Nevertheless, sensitivity can be used as a practical means of identifying and rejecting poorly constrained parts of the inversion models (and in the case of the A5 Block has been used to identify a maximum depth of reliable investigation and to reject poor model solutions in high-fly areas, as discussed in Sections 4 and 5).

Principal Component Analysis Filter

Electromagnetic noise levels are relatively high across many parts of Ireland, originating from multiple cultural noise sources such as power-lines, gas pipelines, towns, industrial centres, farms and dwellings, and have a detrimental effect on the EM response data, particularly at the low 0.9 and 3 kHz transmission frequencies. One particularly useful utility within the *aempy* toolbox is a noise rejection filter based on a Principal Component Analysis (PCA) and decomposition of the EM response data. In this approach, the EM dataset is reconstructed using the strongest and most coherent principal components only, with the weaker principal components (noise) rejected. Previous applications of the approach to airborne EM data (Reninger *et al.*, 2011; Minsley *et al.*, 2012) have illustrated good success in reducing noise contamination and in imposing regularity (consistency) on the data.

In *aempy*, the PCA is based on the singular value decomposition (SVD) (Lanczos, 1961; Golub and van Loan, 1996) of the data observation matrix, D , which has n_{data} rows and n_{site} columns. After removing the average of the rows, matrix D can be decomposed into an orthonormal set of basis functions using the SVD:

$$D = USV^T \quad (3)$$

where U and V are unitary matrices, and S is diagonal and contains the singular values in decreasing sequence. Choosing the k largest values in S and truncating the matrices correspondingly, an approximate matrix D' is obtained, which contains only the coherent components of D . Matrix D' is thus an output filtered (de-noised) version of the input data of matrix D .

In the context of Tellus data, the number of data rows in matrix D is equal to eight (in-phase and quadrature components for 4 frequencies) and as the filter is applied on a



line-by-line basis in *aempy*, the number of site columns in matrix D is equal to the number of sites on the flight line. Choice of an optimal value for k , the number of singular values to be retained in the reconstructed (filtered) data, is considered in Section 3 below.



3. Inversion Parameter Testing

Three A5 Block data subsets (Figures 3.1 and 3.2) were used to test several aspects of the inversion workflow and to test the parameter settings that control the *aempy* Tikhonov-type 1-D inversion:

- i. **Test Dataset A:** Approximately 14 km long sections at the southern ends of 25 adjacent lines: L5274 (west) to L5298 (east). Approximately 2,200 sites on each line.
- ii. **Test Dataset B:** A further subset of Dataset A, consisting of three lines: L5285 (west), L5286 and L5287 (east), with 2,185, 2,248 and 2,224 sites on each line respectively.
- iii. **Test Dataset C:** An approximately 3.7 km long section on line L5285, with 617 sites on the line.

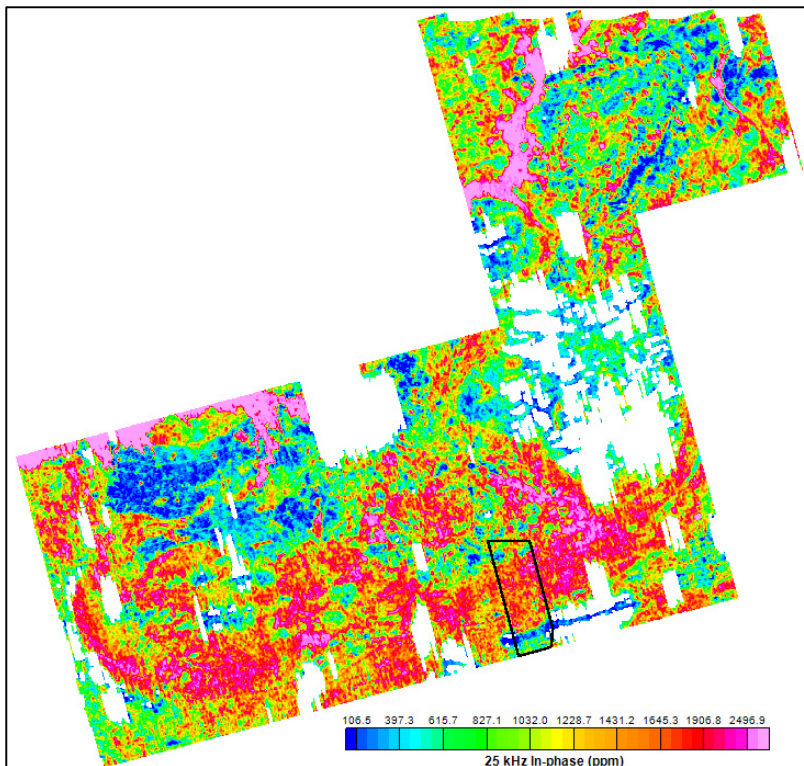


Figure 3.1: Data area (black polygon) used for inversion parameter tests, shown against 25 kHz in-phase data grid. The polygon contains 25 flight lines from L5274 (west) to L5298 (east). Long axis of polygon is approximately 14 km in length. Detail shown in Figure 3.2. The 25 kHz In-phase data are blanked where flight clearance > 100 m (for display only, not for inversion).



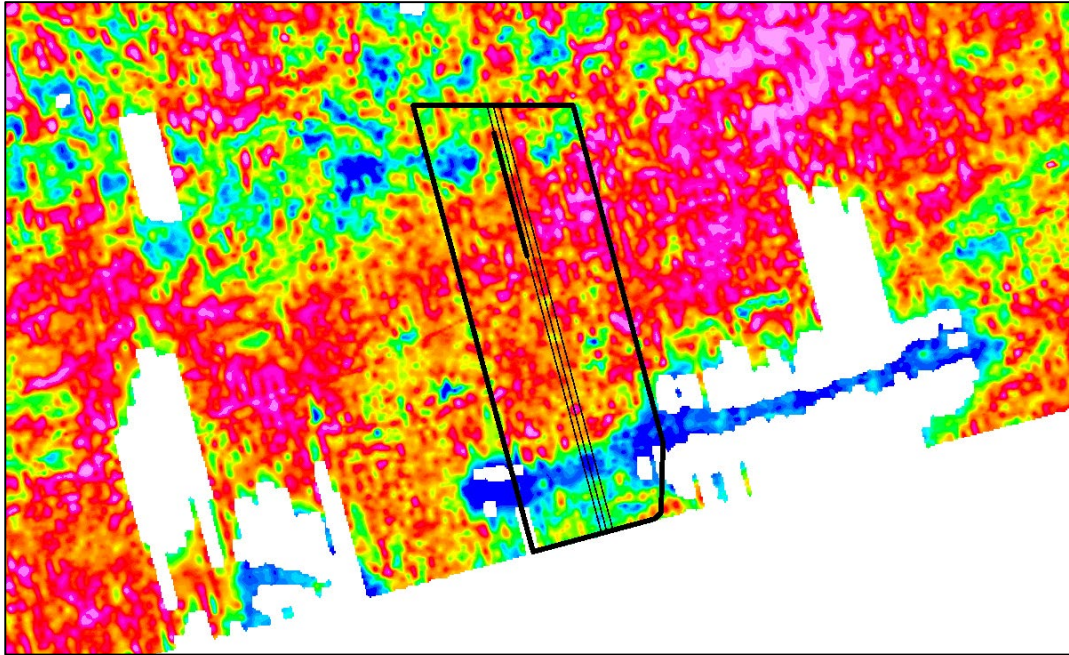


Figure 3.2: Detail of data subsets used for parameter testing, shown against 25 kHz in-phase data grid. Three data subsets (A, B and C) were used variously for different tests: (A) black polygon shows area containing ~14 km long portions of 25 flight lines from L5274 (west) to L5298 (east), (B) thin lines show three central flight lines, L5285 (west), L5286 and L5287 (east) and (C) thicker black line shows ~3.7 km long test portion of L5285. The 25 kHz In-phase data are blanked where flight clearance > 100 m (for display only, not for inversion).

A range of inversion tests and runs were carried out (Table 3.1.) to examine variously the following aspects of the inversion workflow, which are expanded on in more detail in the sections below:

- i. Laser altimeter (clearance) smoothing.
- ii. Application of Principal Component Analysis noise-rejection filter.
- iii. Fully independent 1-D inversion of each site versus non-independent 1-D inversion (i.e., the latter using the previous site's model as the *a priori* (starting) model for current site).
- iv. Single line direction, non-independent inversion models versus forward and reverse line direction model averaging.
- v. Regularisation parameters for Tikhonov-type inversion: τ_0 (closeness to starting model) and τ_1 (model smoothness).
- vi. EM data component errors (for in-phase and quadrature for each frequency independently).



Table 3.1: Summary of inversion runs to test aspects of the inversion strategy and to identify optimum inversion regularisation parameters. The final A5 delivery dataset used for the tests is [GSI___18.IRL_DLV2123_FEM.xyz], the same as used for the production inversion. All tests, except for test No. 2, were run with 35 layer 1-D models, with a shallowest layer thickness of 2 m increasing logarithmically (\log_{10}) with depth to a final layer thickness of 10 m. Test No. 2 used 30 layers and shallowest and deepest layers of 2 m and 5 m respectively. Test datasets A, B and C are described in the text above. Data errors in the table are ordered as follows (where P is in-phase and Q quadrature, followed by the frequency in kHz): P09, P3, P12, P25, Q09, Q3, Q12, Q25. The FRA strategy (short for “forward-reverse-average” strategy) refers to running non-independent inversions in both line directions, and deriving an average model from the two model solutions at each site, as well as computing the differences between the two models for quality control purposes.

Test no.	Test dataset	Low-pass filter (20 FID) applied to clearance	PCA ($k=3$) filter applied	Indep. Models	Strategy	Data errors (ppm)	τ_0	τ_1	No. of sites	Comment
1	B	No	No	No	FRA	All 60.0	0.01	7.0	6,657	Initial inversion to test input data format and FRA strategy coding.
2	C	No	No	No	Fwd. only	All 60.0	0.01	1 - 100 (40 tests)	617	Tau1 test, with Tau0=0.01. Initial test of automated Python script for tau parameter testing.
3	C	No	No	No	Fwd. only	All 60.0	0.01	1 - 100 (40 tests)	617	Tau1 test, with Tau0=0.01.
4	C	No	No	No	Fwd. only	All 60.0	0.1	1 - 100 (40 tests)	617	Tau1 test, with Tau0=0.1.
5	C	No	No	No	Fwd. only	All 60.0	0.001 - 1 (60 tests)	7.4438	617	Tau0 test, with Tau1=7.4438.
6	C	No	No	Yes	Indep. models	All 60.0	0.1	1 - 100 (40 tests)	617	Tau1 test, with Tau0=0.1, independent models.
7	C	No	Yes	No	Fwd. only	All 60.0	0.1	1 - 100 (40 tests)	617	Tau1 test, with Tau0=0.1, Npac3 filtered data.

8	C	No	No	No	Fwd. only	54.0, 65.4, 79.4, 116.8, 54.0, 52.2, 69.3, 90.0	0.1	1 - 100 (40 tests)	617	Tau1 test, with Tau0=0.1, using newly defined data errors (Error-set 4) for each component.
9	C	No	Yes	No	Fwd. only	54.0, 65.4, 79.4, 116.8, 54.0, 52.2, 69.3, 90.0	0.1	1 - 100 (40 tests)	617	Tau1 test, with Tau0=0.1, Npac3 filtered data, using newly defined data errors (Error-set 4) for each component.
10	B	No	Yes	No	FRA	All 60.0	0.01	5.0	6,657	Test inversion, Npca3 filtered data, FRA strategy.
11	C	No	Yes	No	Fwd. only	All 60.0	0.01	1 - 100 (40 tests)	617	Tau1 test, with Tau0=0.01, Npca3 filtered data.
12	C	No	Yes	No	Fwd. only	All 60.0	0.001 - 1 (60 tests)	7.4438	617	Tau0 test, with Tau1=7.4438, Npca3 filtered data.
13	A	No	Yes	No	FRA	All 60.0	0.01	6.0	~55,000	Inversion, Npca3 filtered data, FRA strategy.
14	A	No	No	No	FRA	All 60.0	0.01	7.5	~55,000	Inversion, FRA strategy.
15	C	No	No	Yes	Indep. models	All 60.0	0.001 - 1 (60 tests)	10.6081	617	Tau0 test, with Tau1=10.6081, indep. models.
16	C	Yes	No	No	Fwd. only	All 60.0	0.01	1 - 100 (40 tests)	617	Tau1 test, with Tau0=0.01, clearance LP filtered.
17	C	Yes	Yes	No	Fwd. only	All 60.0	0.01	1 - 100 (40 tests)	617	Tau1 test, with Tau0=0.01, with Npca3 filtered data, clearance LP filtered.

18	A	Yes	Yes	No	FRA	All 60.0	0.01	6.0	~55,000	Data error test - Error-set 0 ("unweighted" errors). Inversion, using FRA strategy, best Tau0 and Tau1 values, Npca3 filtered data, clearance LP filtered.
19	A	Yes	Yes	No	FRA	70.0, 70.0, 50.0, 50.0, 70.0, 70.0, 50.0, 50.0	0.01	6.0	~55,000	Data error test - Error-set 1. Inversion using FRA strategy, best Tau0 and Tau1 values, Npca3 filtered data, clearance LP filtered.
20	A	Yes	Yes	No	FRA	70.0, 60.0, 50.0, 40.0, 70.0, 60.0, 50.0, 40.0	0.01	6.0	~55,000	Data error test - Error-set 2. Inversion using FRA strategy, best Tau0 and Tau1 values, Npca3 filtered data, clearance LP filtered.
21	A	Yes	Yes	No	FRA	54.11, 27.56, 68.11, 46.10, 54.68, 20.95, 60.71, 28.55	0.01	6.0	~55,000	Data error test - Error-set 3. Inversion using FRA strategy, best Tau0 and Tau1 values, Npca3 filtered data, clearance LP filtered.
22	A	Yes	Yes	No	FRA	54.0, 65.4, 79.4, 116.8, 54.0, 52.2, 69.3, 90.00	0.01	6.0	~55,000	Data error test - Error-set 4. Inversion using FRA strategy, best Tau0 and Tau1 values, Npca3 filtered data, clearance LP filtered.
23	A	Yes	Yes	No	FRA	54.0, 65.4, 79.4, 100.0, 54.0, 52.2, 69.3, 70.00	0.01	6.0	~55,000	Data error test - Error-set 5. Inversion using FRA strategy, best Tau0 and Tau1 values, Npca3 filtered data, clearance LP filtered.

Laser Altimeter (Clearance) Smoothing

Aircraft clearance data (aircraft height above ground level) are a required input into the *aempy* inversion code (as the amplitudes of EM responses are strongly dependent on EM sensor height above ground level). In the case of the contractor-delivered EM dataset, clearance data are derived from the aircraft's laser altimeter and are subject to noise spikes (as shown in the upper panel of Figure 3.3) that are largely the result of unreliable laser reflectance when flying over areas of thick, tall or variable vegetation cover.

The analysis that follows uses the example of L5285 from Dataset Set C and takes inversion results from Tests 11 and 17 (Table 3.1). Inversions from the two tests are identical in their parameters, except for Test 11 using raw laser altimeter data and Test 17 using filtered altimeter data. Uncorrected (raw) laser altimeter data, as input into *aempy*, were found to produce spurious 1-D inversion models as illustrated by the "spikes" in the model cross-section of Figure 3.4 (upper panel). As surface topography referenced to sea-level, *DEM*, is derived from the clearance data:

$$DEM = MSLHGT - CLEARANCE \quad (4)$$

where *MSLHGT* is the aircraft GPS *Z* coordinate referenced to sea-level, spikes in the clearance data also translate into spikes in the topography model, as apparent in Figure 3.4.

Confirmation that the laser altimeter spikes do not reflect real, sudden changes in flight altitude is provided by the observation in Figure 3.3 that there are no changes in the EM responses coincident with the altimeter spikes. Two filters (low-pass and non-linear) and a range of filter settings were tested for spike removal in the altimeter data. A 20-fiducial (~120 m wavelength) low-pass filter was found to provide optimal results (Figure 3.3) – producing a clearance channel with wavelength variations commensurate with the observed EM response data and with minimal artefacts in the vicinity of clearance spikes. A shorter low-pass filter wavelength length (e.g., 10 fid) did not effectively remove many of the observed spikes in the clearance data.

A 20-fiducial low-pass filter was therefore applied to the clearance data prior to production inversion of Block A5.



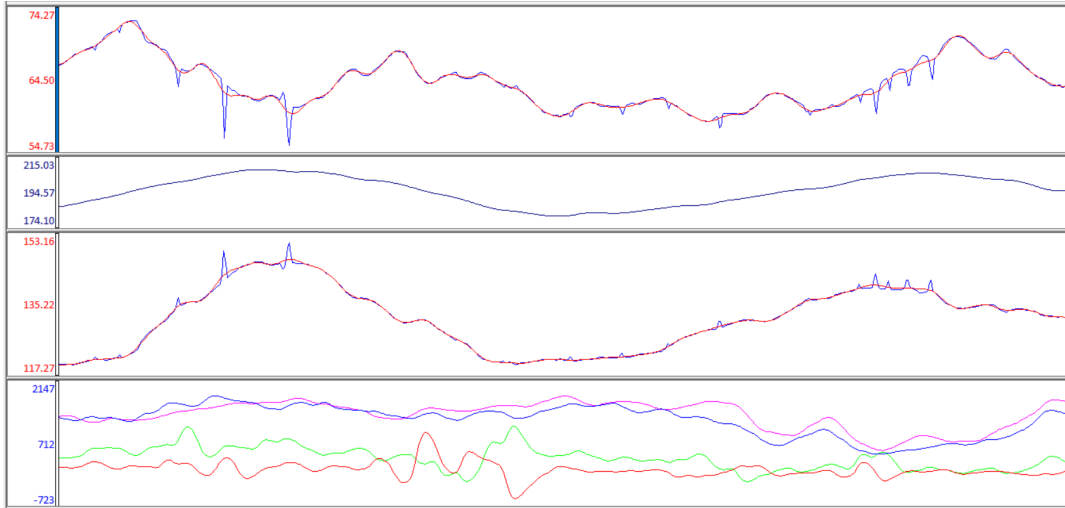
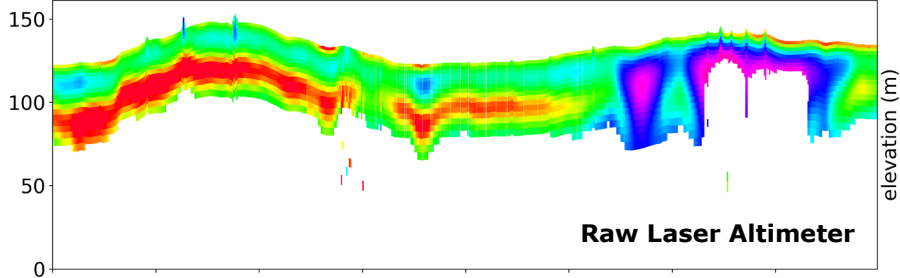


Figure 3.3: Line L5285 profile display (3.7 km long section, Test Dataset C) showing: (top panel) raw clearance (laser altimeter) data (blue) and low-pass filtered (20-fiducial) clearance data (red); (upper middle panel) aircraft GPS Z coordinate data referenced to sea-level; (lower middle panel) DEM referenced to sea-level calculated from raw clearance data (blue) and low-pass filtered clearance data (red); (bottom panel) in-phase responses at 0.9, 3, 12 and 25 kHz (red, green, blue and purple respectively). North is to the right-hand side of the profiles.

Block A5 L5285.0.lev: Npca3, trms2=1e-5, t0=0.01, t1=5.87801, Lowsens=0.001



Block A5 L5285.0.lev: clearlp, Npca3, trms2=1e-5, t0=0.01, t1=5.87801, Lowsens=0.001

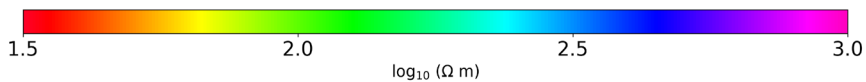
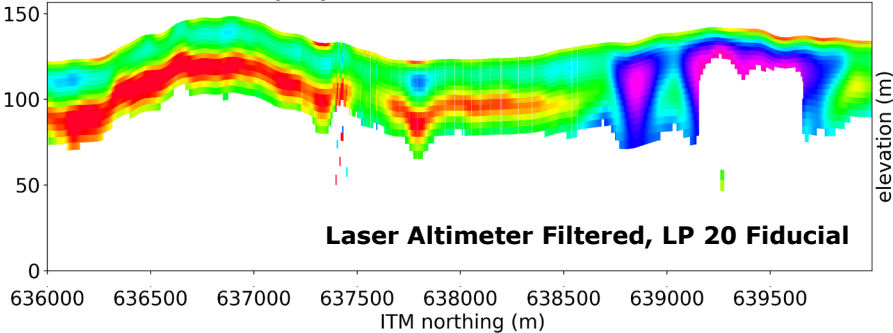


Figure 3.4: Line L5285 (Test Dataset C): Comparison between EM inversion resistivity models computed using (top) raw laser altimeter data and (bottom) low-pass filtered (20-fiducial) laser altimeter data as input. The 2-D section shown is the result of plotting along the profile the 1-D resistivity models computed at each site. Spikes in the resistivity model (and in the constructed topographic surface) are apparent in the upper figure due to noise spikes in the laser altimeter data. Colour scale used has conductive bodies shown in red and resistive bodies in blues/purples. Models are blanked where normalised model sensitivity is less than a defined



threshold of 0.001 (the normalisation factor used is the maximum sensitivity for the profile, determined separately for each profile). North is to the right-hand side of the profiles.

Principal Component Analysis Noise-Rejection Filter

The Principal Component Analysis filter, as described in Section 2 above, is applied prior to EM inversion with the objective of reducing noise and imposing regularity and consistency on the EM response data. In decomposing the EM data into amplitude-ordered singular values (principal components), the critical decision in reconstructing, and thereby effectively filtering, the data lies in the selection of the cut-off between significant, coherent principal components (which will be retained) and incoherent, insignificant principal components (noise, which will be rejected) – i.e., choosing the value for k , where the largest k values in the singular value matrix S are retained (see Section 2).

An examination of the EM data recorded at multiple flight heights over the Tellus Bundoran Test Line (Kiyani *et al.*, in review) indicates that most of the coherent data are present in the first two principal components (or singular values) (Figure 3.5). In the upper panel of Figure 3.5, it is apparent that all singular value amplitudes are low for flight heights equal to and greater than 120 m; that significant amplitudes are found in singular values 1 and 2 for flight heights of 90 m and lower; and that significant amplitudes are found in singular values 1, 2 and 3 for flight heights of 80 m and lower.

The effect of applying the PCA filter to the EM data can be assessed by examining the differences between the input and filtered data. In the lower panel of Figure 3.5, a comparison is made using the root-mean-square error (or difference) between the input and filtered data, as a function of the number of singular values (principal components) retained in the data reconstruction. In this lower panel, for example, the data plotted at #SV = 3 correspond with the RMS error between the recorded (input) data and the data reconstructed using singular values 1, 2 and 3 only. Retaining all eight singular values (#SV = 8) reconstructs the input data exactly, returning an RMS error of zero. Whether the filtered data satisfactorily capture the coherent signal in the recorded data depends on the data errors estimated for the recorded data themselves. Given that the average data error for all eight EM data components is unlikely to be less than 40 ppm (as discussed in more detail in the “EM Component Data Errors” section below), it is apparent in Figure 3.5 (lower panel) that only singular values 1 and 2 are required to



reconstruct the data to within the data observational error and that higher singular values are essentially contributing noise.

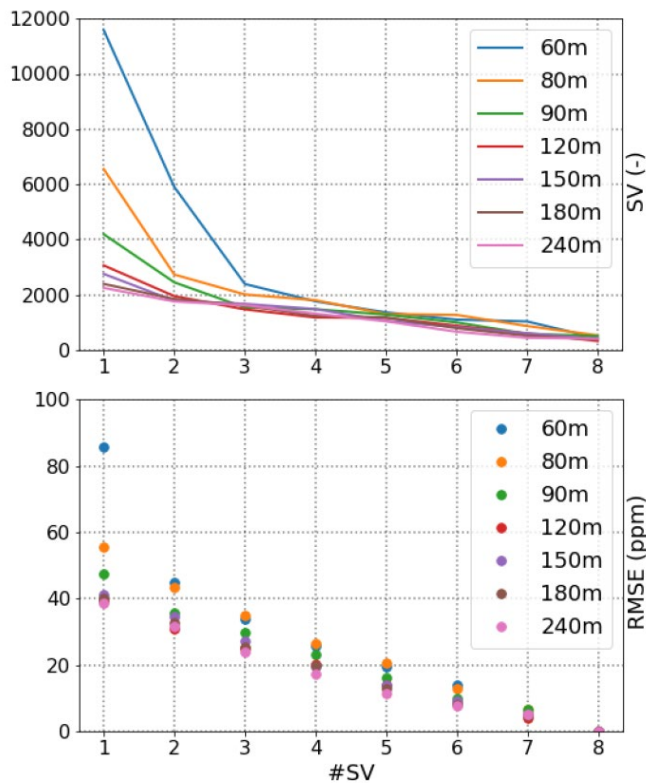


Figure 3.5: Summary of Singular Value Decomposition (SVD) analysis results for Tellus Bundoran Test Line data for seven flight altitudes, flown in 2015. (Upper panel) shows singular value amplitude (SV) for each singular value (#SV). (Lower panel) shows the root-mean-square error (RMSE) between the observed data and the reconstructed data versus singular value number (#SV). In the lower panel, for example, the data plotted at #SV = 3 correspond with the RMS error between the recorded data and the reconstructed data using singular values 1, 2 and 3 (i.e., using $k = 3$). From Kiyani et al. (in review).

In taking a conservative approach in applying the PCA filter to the data of Block A5, principal components 1, 2 and 3 have been used in the data reconstruction (i.e., using $k = 3$), reducing the possibility of rejecting some coherent geological signal and allowing for lower than average noise levels in some of the eight EM data components. Figure 3.6 compares the recorded (input) data and PCA filtered data for $k = 3$ for Line L5285 from Test Dataset C (this filter, for brevity and convenience, is referred to as the “Npca3” filter in the text). The most obvious impacts of the Npca3 filter observed in the L5285 data are the removal of several high-amplitude (noise) spikes in the low frequency, in-phase 0.9



and 3 kHz data components and a general smoothing of the data for all eight data components.

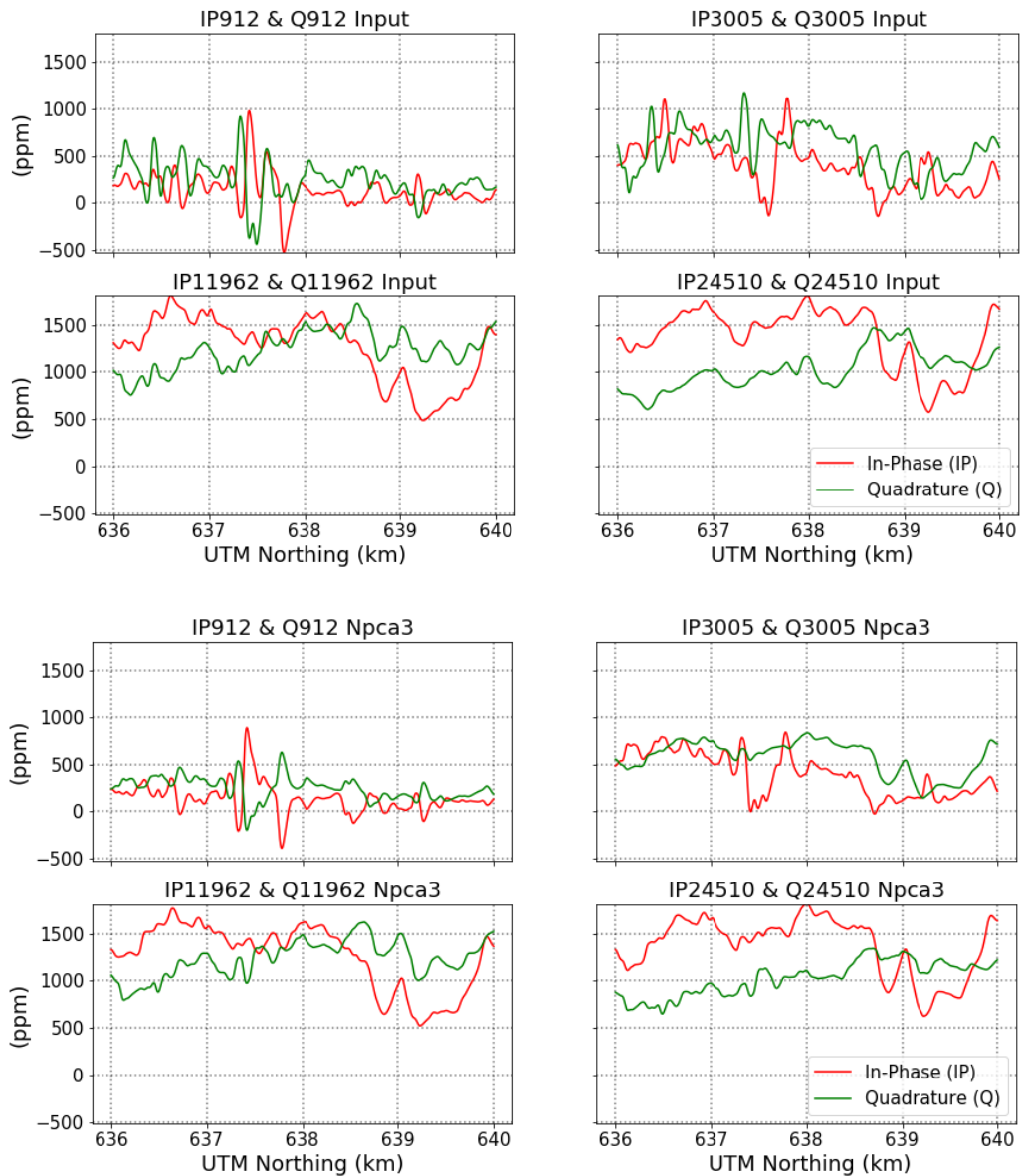


Figure 3.6: Line L5285 (Test Dataset C): (Upper four panels): recorded (input) data for in-phase (IP) and quadrature (Q) components for 912, 3,005, 11,962 and 24,510 Hz frequencies. (Lower four panels): PCA filtered data ($k = 3$, Npca3) for in-phase (IP) and quadrature (Q) components for 912, 3,005, 11,962 and 24,510 Hz frequencies. North is to the right-hand side of the profiles.

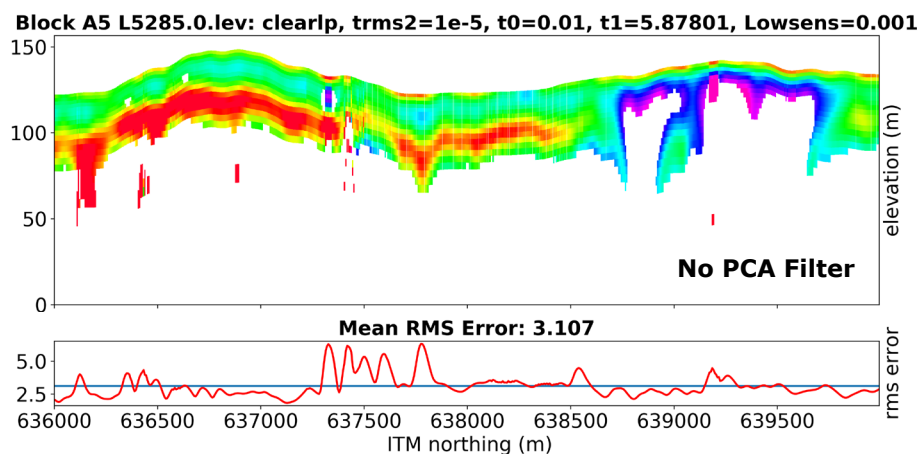
Figure 3.7 compares *aempy* inversion model results for L5285 (Test Dataset Set C) derived using the unfiltered EM data of Figure 3.6 (inversion Test 16, Table 3.1) and the Npca3 filtered data (inversion Test 17). Except for the application of the Npca3 filter, the



two test inversions are identical in their parameters. The unfiltered and Npca3 filtered data models return mean profile RMS errors (misfits) between the observed and predicted responses of 3.107 and 2.731 respectively. In both cases, but particularly for the Npca3 model, the individual site RMS errors are lower than the line average over much of the profile – a result of the poor model fits over the 500 m section between ITM Y coordinates 637,300 – 637,800 m significantly increasing the average error. Note that the RMS errors reported by *aempy* are normalised by the data errors – specified as 60.0 ppm for all data components in the case of these two tests – and an RMS error = 1 would indicate a fitting of the observed data to within data error.

In comparing the two models of Figure 3.7, the Npca3 filtered result shows generally improved model continuity. There is no evidence of loss of geological detail with respect to the unfiltered result, indicating that the Npca3 filter has not removed coherent geological signal from the EM data. Improved data and model stability is also indicated by the smoother RMS misfit profile for the Npca3 filtered data. The absence of significant differences in the main features recovered in the two models suggests that the reduction in the average RMS error for the Npca3 model is primarily due to the removal of noise in the data (i.e., noise that can't be fit by the inversion modelling in the unfiltered data).

On the basis of the above results, the Npca3 filter (PCA filter, with $k = 3$) was therefore applied to EM response data prior to production inversion of Block A5.



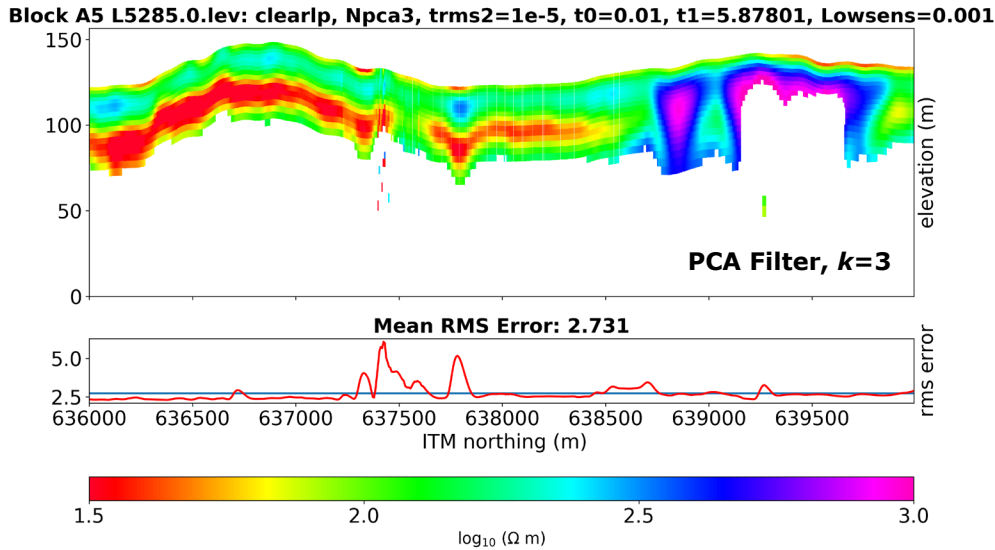


Figure 3.7: Line L5285 (Test Dataset C): Comparison between EM inversion models computed (top) without PCA filter and (bottom) with PCA filter, retaining first three principal components. Profiles of RMS error at each site are shown below the model sections (horizontal blue line shows the mean RMS error for the profile). In both inversions, flight clearance data are low-pass filtered (20-fiducial). Colour scale used has conductive bodies shown in red and resistive bodies in blues/purples. Models are blanked where normalised model sensitivity is less than a defined threshold of 0.001 (the normalisation factor used is the maximum sensitivity for the profile, determined separately for each profile). North is to the right-hand side of the profiles.

Independent versus Non-independent Inversion

The *aempy* Tikhonov-type inversion code provides two options for the *a priori* (starting) model used at each EM measurement site (keeping in mind that the 1-D inversions are run on a line-by-line basis):

- i. a half-space with a user defined resistivity value, referred to here as **“independent”** inversion, and
- ii. the previous site’s resistivity model (with the starting model for the first site on the line being a half-space with a user defined resistivity value), referred to here as **“non-independent”** inversion.

Similar to other geophysical methods, EM modelling is subject to the concept of equivalence – in which different possible model solutions can satisfy equally well the observed EM response data, to within data error. The EM method is particularly sensitive to conductive subsurface bodies, specifically to their conductance (the conductivity-thickness product), and is therefore particularly subject to equivalence in



the modelling of conductors (i.e., a thinner, more conductive body producing an equivalent EM response to a thicker, less conductive body).

In running independent inversions at each site, there is no restriction placed on the possibility of adjacent sites converging on different, but equivalent, model solutions, potentially leading to discontinuous or blocky resistivity model sections along flight lines. The use of the previous site's model as the starting model, as done in the non-independent inversion, attempts to "nudge" the inversion towards convergence on a model that does not deviate dramatically from the previous site's model, unless required to do so by the EM data. Choice of the inversion regularisation parameter τ_0 , which controls the freedom of divergence from the starting model, provides a means of controlling how rapidly site-to-site inversions can respond to lateral changes in geology when using non-independent modelling (see the "Inversion Regularisation Parameters" section below for further discussion).

Test inversions carried out confirm a tendency for independent inversions to produce less continuous model sections along flight lines - with a certain "blockiness" apparent as model solutions transition from one set of similar models to a different (but equivalent) set of models along the line – as illustrated in the example of L5285 (from Test Dataset C) in Figure 3.8. The same blockiness is also apparent in the normalised sensitivity section for the independent inversion. The independent inversion result in Figure 3.8 is taken from inversion Test 6 (Table 3.1), where a 100 Ω .m starting model was used, delivering a mean RMS error for the line of 3.292, and the non-independent inversion result from Test 4, where a 100 Ω .m starting model was used for the first site on the line, delivering a mean RMS error of 3.107. The same inversion regularisation parameters were used in both cases.

While independent and non-independent inversions produce models with the same or very similar RMS errors, and which are therefore quantitatively equally valid model solutions, the greater continuity of features in non-independent inversion models is preferred as being more geologically realistic and more interpretable, and **on this basis non-independent inversions were used in the production inversion of Block A5**. Practically, there is some advantage in inversion time or speed in running non-independent inversions, as fewer inversion iterations are generally needed to converge on the final solution. However, this inversion speed advantage is offset by employing



the strategy of modelling each flight line twice, in forward and reverse directions (as discussed further in the section below).

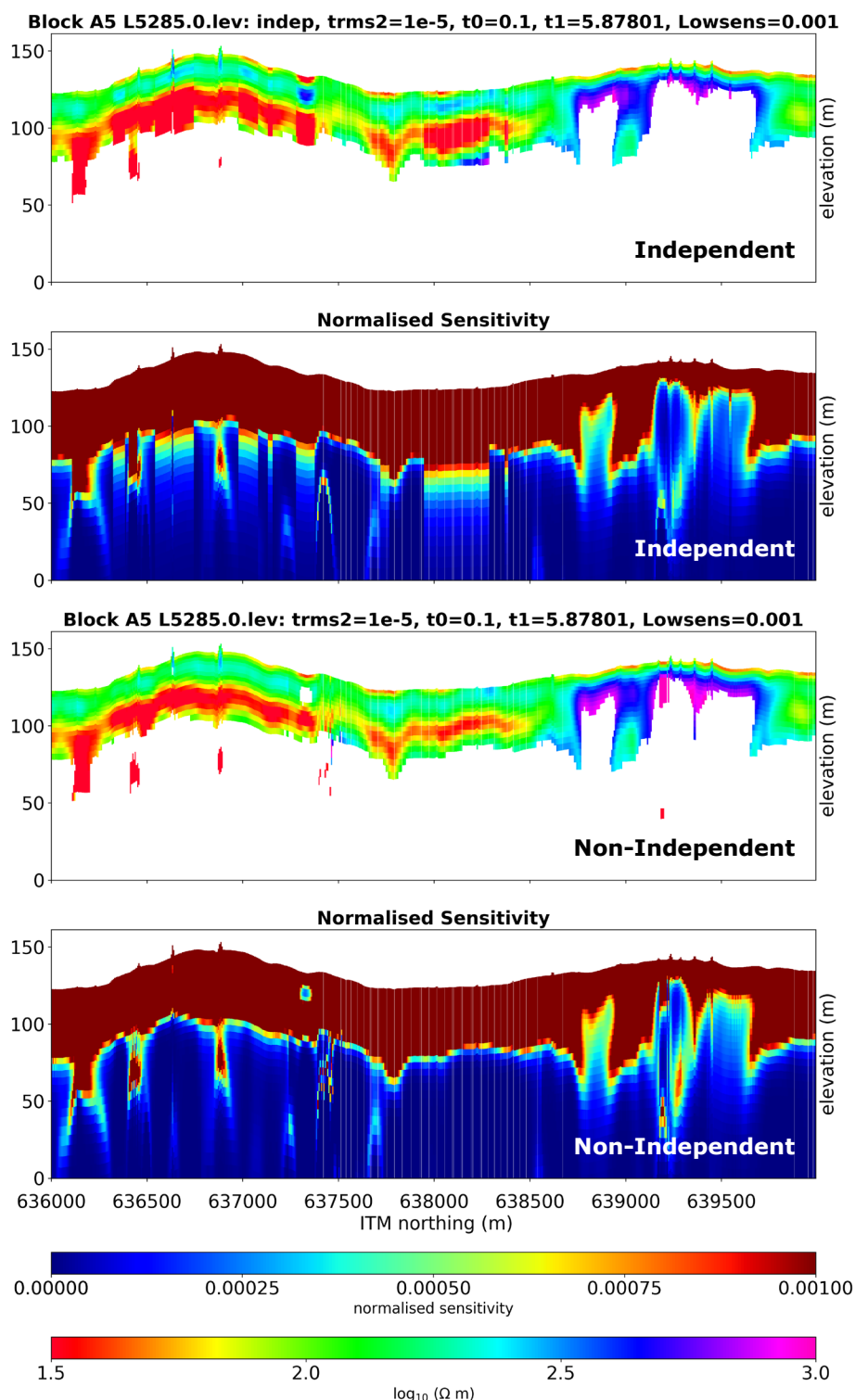


Figure 3.8: Line L5285 (Test Dataset C): Comparison between EM inversion models and normalised sensitivity sections computed (top two panels) using independent modelling (starting model for all sites is a 100 Ωm half-space) and (bottom two panels) non-independent



modelling (starting model for each site is previous site's model, with the starting model for the first site on the line being a 100 $\Omega.m$ half-space). In both inversions, flight clearance data used have not been low-pass filtered and a PCA filter has not been applied. Colour scale used has conductive bodies shown in red and resistive bodies in blues/purples. Models are blanked where normalised model sensitivity is less than a defined threshold of 0.001 (the normalisation factor used is the maximum sensitivity for the profile, determined separately for each profile). North is to the right-hand side of the profiles.

Averaging of Non-independent Inversion Models (FRA Strategy)

Running non-independent inversions (i.e., using the previous site's model as the starting model) raises the possibility that resulting model sections may be somewhat different depending on the line direction in which the inversions are run. It also presents the possibility of running inversions in both line directions, assessing the differences between the two models and deriving an average model from two equally valid model solutions – a strategy referred to here as the “forward-reverse-average” (FRA) strategy.

The FRA strategy is examined below (Figure 3.9) using line L5285 model results from inversion Test 18 (Table 3.1) (Test Dataset A). The inversion data and parameter settings used are as follows: low-pass filter applied to clearance data, Npca3 filter applied to EM component data, regularisation parameters $\tau_0 = 0.01$ and $\tau_1 = 6.0$, and data errors for all EM components = 60.0 ppm. The mean RMS errors for both line directions are identical at 2.448.

While visually there are no significant differences apparent between the forward direction, reverse direction and average model sections in Figure 3.9, the percentage difference section does highlight portions of the model where the solutions might be regarded as less reliable. Note that percentage difference here is the percentage difference between the two models with respect to the average model, and is computed at every model depth location in the subsurface. Sites in the difference section, where large differences are seen throughout the vertical column, are generally coincident with high site RMS errors. In other instances, less stable model solutions (i.e., those solutions with larger differences) are only observed in deeper parts of the model.



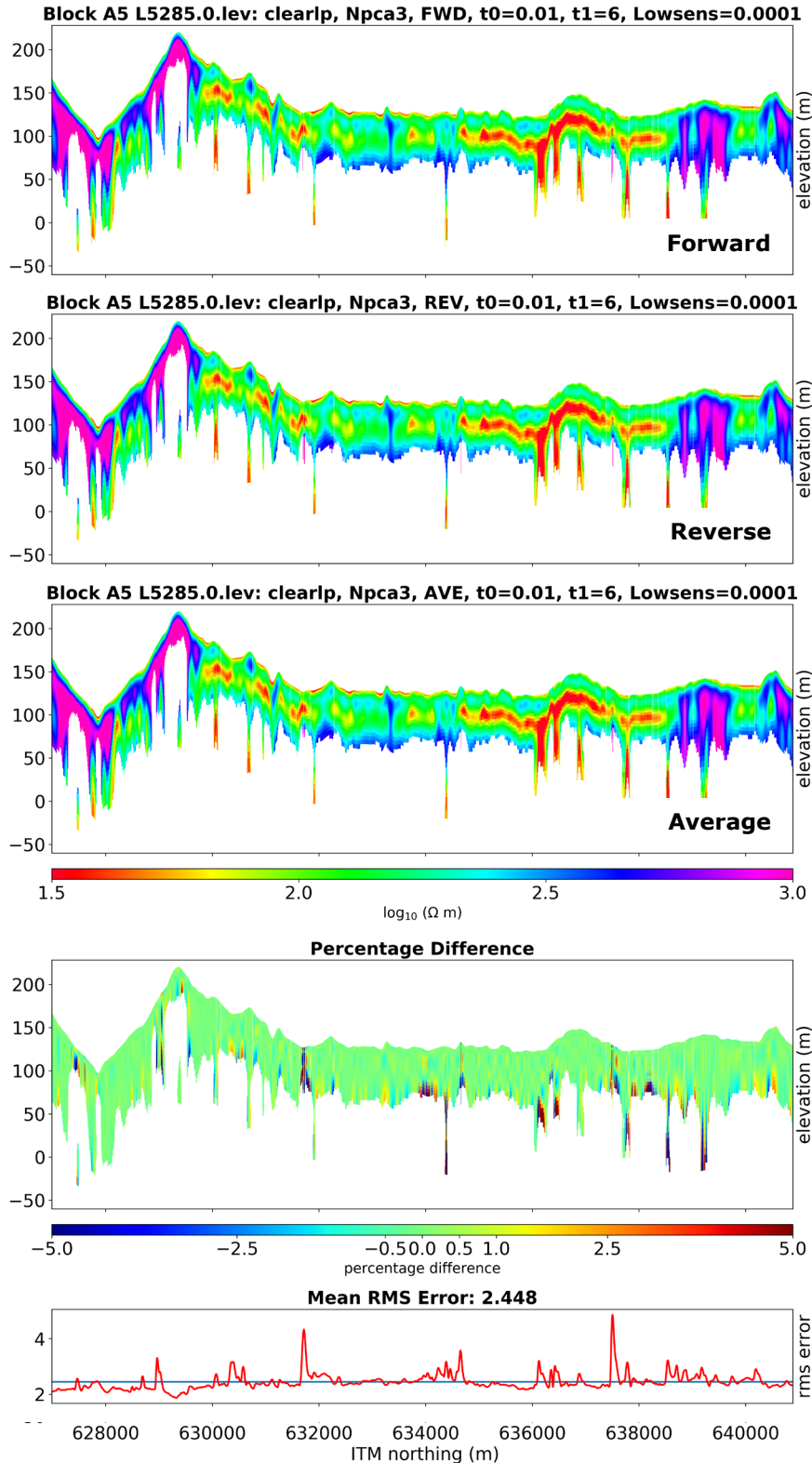


Figure 3.9: Line L5285 (Test Dataset A): Comparison between non-independent inversion models computed (top panel) in a forward direction along the profile and (second panel) in a reverse direction. (Third panel) shows the average of the forward and reverse direction models. (Fourth panel) shows the percentage differences between the two models with respect to the average model and (bottom panel) shows the average RMS error along the profile (i.e., average of forward and reverse direction RMS errors), with horizontal blue line indicating the line average. Models are blanked where normalised model sensitivity is less than a defined



threshold of 0.0001 (the normalisation factor used is the maximum sensitivity for the profile, determined separately for each profile). North is to the right-hand side of the profiles.

The percentage difference parameter provides an opportunity for rejecting poorer, less stable parts of the resistivity model, by defining an acceptable percentage difference threshold. Its application offers a more surgical approach than using site RMS error as a model rejection criterion – the latter rejecting the entire model associated with a site, while the former restricts rejection to specific portions and depths of the model section. The potential for automated, post-inversion model cleaning is seen as perhaps the main advantage of applying the FRA strategy, as the average resistivity models themselves are likely, in most cases, not to be significantly different from single direction inversion models.

The FRA inversion strategy has therefore been adopted for the production inversion of Block A5.

Inversion Regularisation Parameters

The values assigned to each of the two regularisation parameters associated with the *aempy* Tikhonov-type inversion have a particularly strong influence on the shape of the output resistivity models and on the closeness of the fit of the predicted EM responses to the observed responses (i.e., the model RMS error):

- i. **τ_0 parameter:** Controls the closeness of the inversion model to the *a priori* (starting) model (i.e., it controls the freedom to diverge from the starting model). Larger τ_0 values allow less freedom to diverge from the starting model.
- ii. **τ_1 parameter:** Controls the 1-D model smoothness. Larger τ_1 values produce smoother models.

The values that might be assigned to the regularisation parameters depend on the particular characteristics of the EM dataset being modelled (e.g., frequencies used and data errors) and on the parameterisation of the model space (e.g., number of layers, layer thicknesses and starting model). It is therefore necessary to run appropriate tests to determine the optimal values for parameters τ_0 and τ_1 for the dataset and inversion scheme being used.



Twelve different tests (Table 3.1) were carried out, using Test Dataset C, to assess the effects of variation of τ_0 (three tests) and τ_1 (nine tests) on the output resistivity models and output RMS errors, for various different inversion inputs and schemes: independent and non-independent inversions, clearance data low-pass filtered and not filtered, and EM component data Npca3 filtered and not filtered. The tests evaluate τ_0 in the range 0.001 – 1 (60 tests in total) and τ_1 in the range 1 – 100 (40 tests in total), with logarithmic increments between each tau value tested. A task-specific *aempy* script was used to automate the tau test runs. All tests were run using data errors of 60.0 ppm for all eight EM components, except for Tests 8 and 9, which used a set of errors based on an analysis of the A5 Block high-fly data (Error-set 4, as defined in Table 3.1 and discussed below in the “EM Component Data Errors” section) in which different error values, in the range 52.2 – 119.8 ppm, are assigned variously to each of the EM components. All tests were run with unsmoothed clearance data, except for Test 17, where the clearance data were smoothed with a 20-fiducial low-pass filter.

Figures 3.10 and 3.11 illustrate the tau versus model RMS error results (“L-curves”) for a number of different test runs. The markedly different L-curve shapes, particularly for the τ_1 tests (Figure 3.10), illustrate the importance of running the tests using the same inversion scheme and data errors as planned for production inversion. While the non-independent inversion tests all deliver a minimum RMS error τ_1 value around 5.0 – 6.0, the independent inversion test (Test 6) shows a minimum RMS value at around $\tau_1 = 10.6$. Changing the data errors assigned to each of the eight EM data components, as for Test 9 (using Error-set 4, defined in the following section), has dramatically reduced the sensitivity of model RMS error to τ_1 , producing a very flat L-curve with a minimum RMS error τ_1 value of around 2.6. Note that the RMS errors for Test 9 are lower because the Error-set 4 data errors are on average higher than the 60.0 ppm used for the other tests (and RMS errors are normalised by the data error).



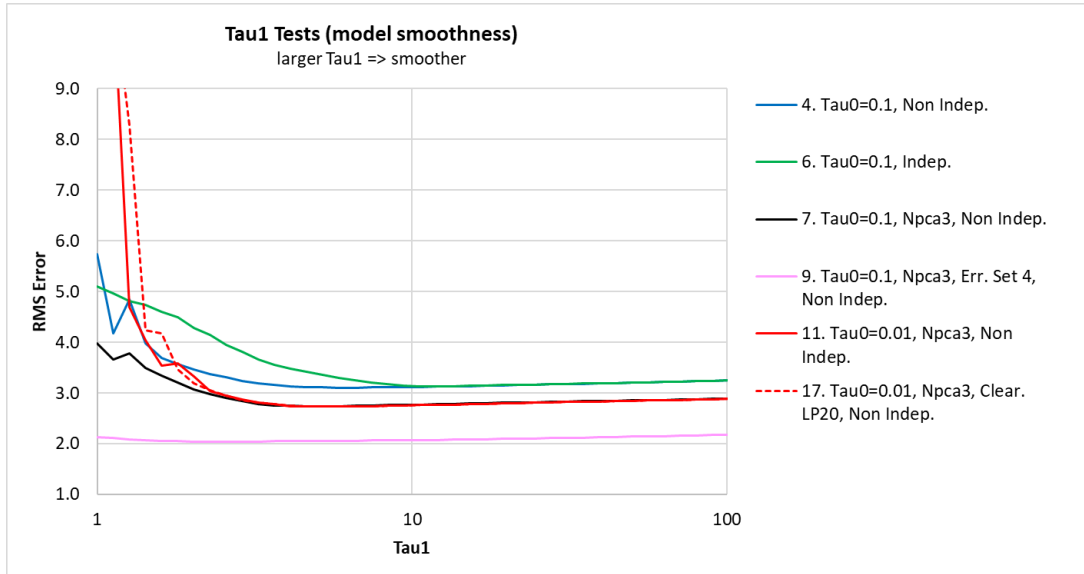


Figure 3.10: τ_1 versus RMS error curves (L-curves) for a range of different τ_1 tests (Test Dataset C). Primary details and settings for the tests are annotated in the legend and test numbers correspond with Table 3.1.

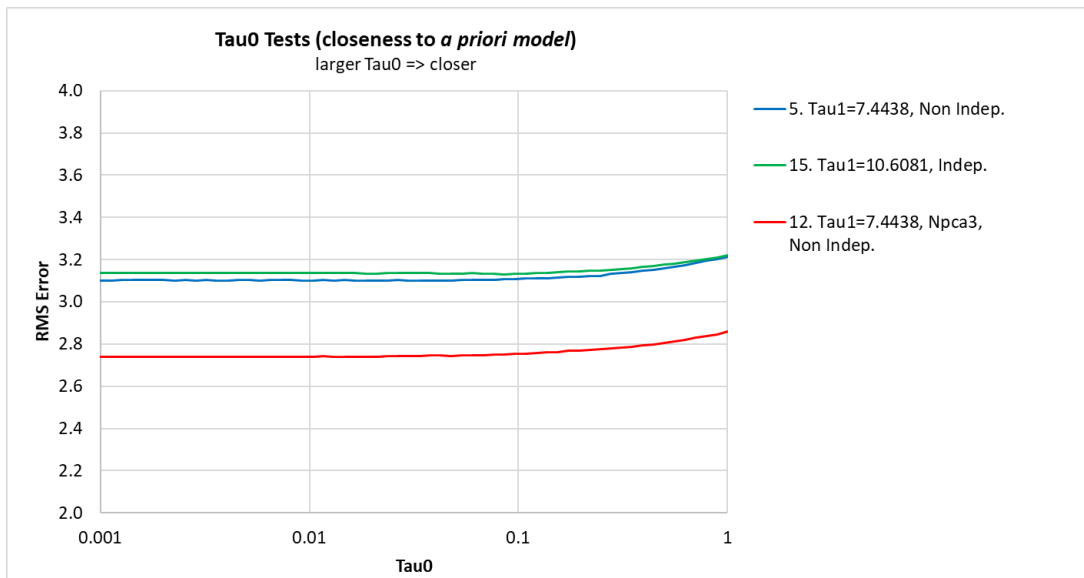


Figure 3.11: τ_0 versus RMS error curves (L-curves) for a range of different τ_0 tests (Test Dataset C). Primary details and settings for the tests are annotated in the legend and test numbers correspond with Table 3.1.

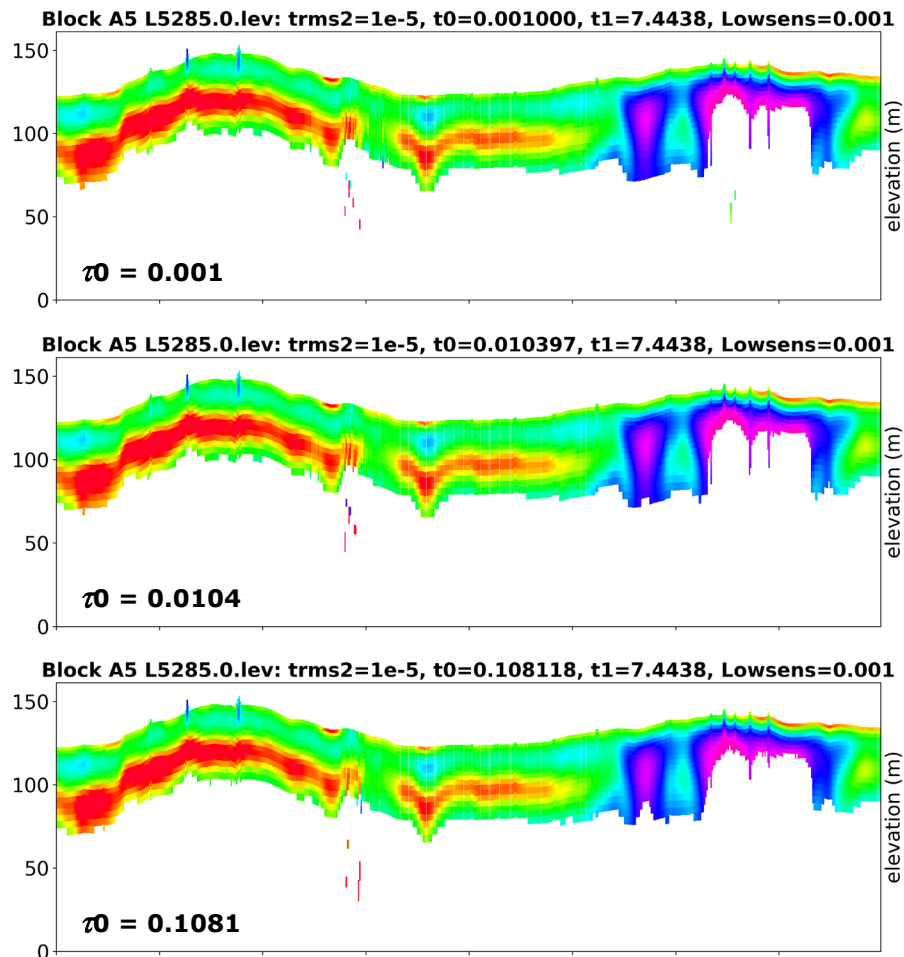
From a purely quantitative point of view, the best tau value is that providing the lowest RMS error model solution. For tests that best replicate the production inversion strategy used for Block A5 (Test 17 for τ_1 , Figure 3.10 and Test 12 for τ_0 , Figure 3.11), the minimum RMS error tau values are: $\tau_0 = 0.002018$ (RMS error = 2.738) and $\tau_1 = 5.87801$ (RMS error = 2.731).



For the production inversion of Block A5, the following tau values were adopted:

$$\tau_0 = 0.01 \text{ and } \tau_1 = 6.0$$

A strategic decision was taken to use the somewhat larger τ_0 value of 0.01 for production inversion (which in Test 12 corresponds with an almost negligibly different RMS error of 2.740), rather than use the minimum RMS error τ_0 value of 0.002, so as to encourage a moderately stronger adherence to the starting model (i.e., the previous site's model) and to (potentially) enhance model continuity along each flight line. Practically, however, the dependence on τ_0 of the output model "shape" is very weak, particularly in the range of values between 0.001 and 0.1, as illustrated in Figure 3.12.



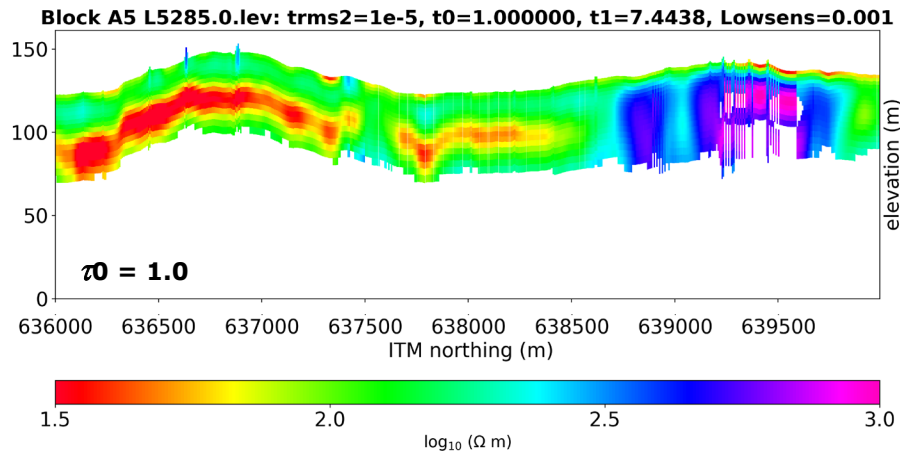


Figure 3.12: τ_0 tests, Line L5285 (Test Dataset C): Comparison of output resistivity models for different inversion τ_0 values, taken from Test 12 (Table 3.1). Figures from top to bottom illustrate results for τ_0 values of 0.001, 0.0104, 0.1081 and 1.0. RMS errors for these models are 2.739, 2.740, 2.755 and 2.858 respectively. A value of $\tau_0 = 0.01$ was selected for production inversion of Block A5. Models are blanked where normalised model sensitivity is less than a defined threshold of 0.001 (the normalisation factor used is the maximum sensitivity for the profile, determined separately for each profile). North is to the right-hand side of the profiles.

The dependence of RMS error and model “shape” on τ_1 is particularly strong (Figure 3.13). Lower τ_1 values produce noticeably sharper models (in a vertical, 1-D sense), but with a strong trade-off against RMS error (i.e., much higher RMS errors than provided by the minimum RMS error τ_1 value). Larger τ_1 values produce much smoother models, with a more moderate trade-off against RMS error (i.e., a moderate increase in RMS error). While the τ_1 value chosen for the production inversion of Block A5 does use the minimum RMS error τ_1 value (providing quantitatively the best fitting models to the data) and visually provides models that have good vertical resolution (i.e., they are judged as not too smooth), other users of Tellus data and the *aempy* software may choose to use different τ_1 values, so as to derive much sharper or smoother models, depending on the geological setting and their modelling objectives.



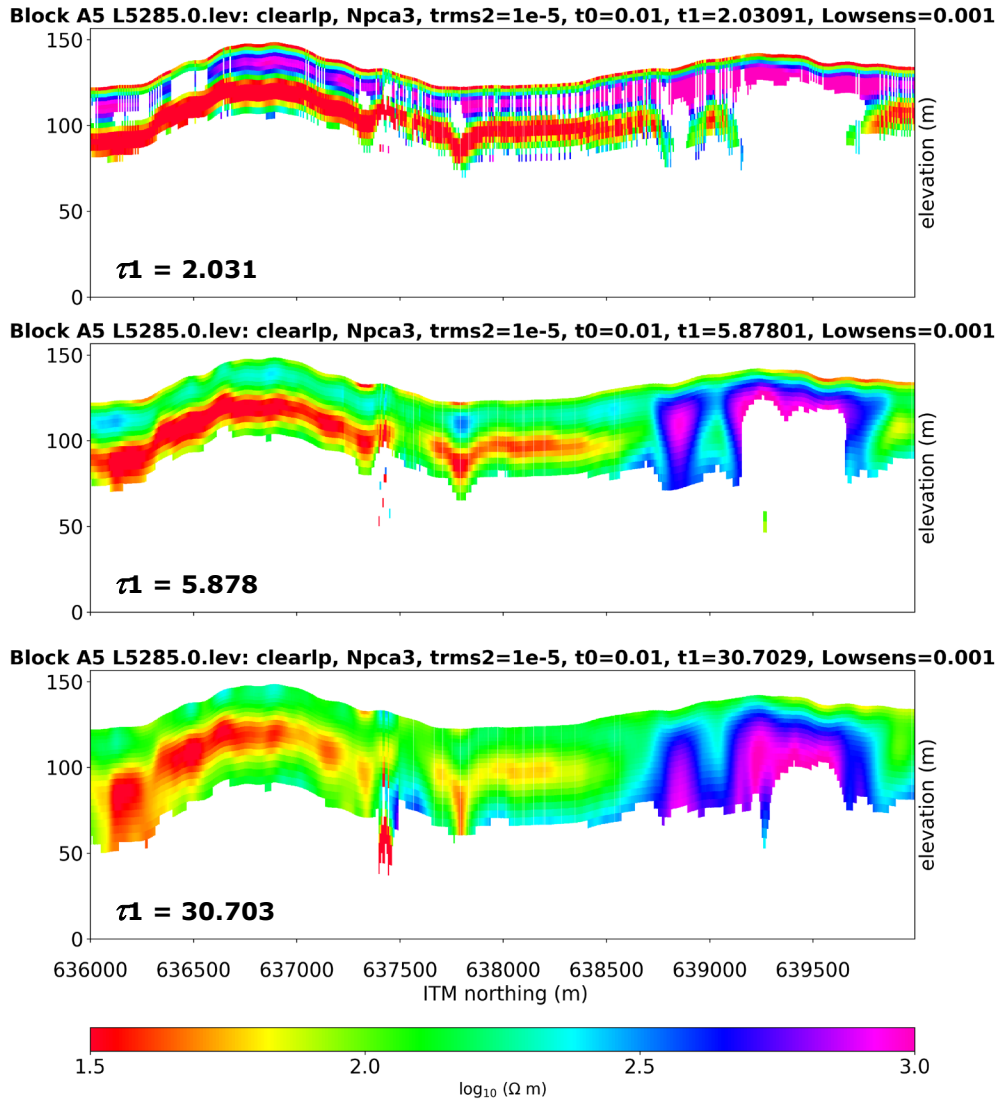


Figure 3.13: τ_1 tests, Line L5285 (Test Dataset C): Comparison of output resistivity models for different inversion τ_1 values, taken from Test 17 (Table 3.1). Figures from top to bottom illustrate results for τ_1 values of 2.031, 5.878 and 30.703. RMS errors for these models are 3.191, 2.731 and 2.823 respectively. A value of $\tau_1 = 6.0$ was selected for production inversion of Block A5. Models are blanked where normalised model sensitivity is less than a defined threshold of 0.001 (the normalisation factor used is the maximum sensitivity for the profile, determined separately for each profile). North is to the right-hand side of the profiles.

The vertical striping in the upper resistive layer in the $\tau_1 = 2.031$ model in Figure 3.13 (upper panel) is a result of the application of a sensitivity-based model blanking, using a normalised sensitivity threshold of 0.001. EM data are relatively insensitive to resistors and the very high resistivities returned in this layer, as a result of the low τ_1 value used, are associated with very low model sensitivities, below the threshold value. The fact that there is strong sensitivity to the conductor below the resistor indicates that the resistor is not a fully unconstrained part of the model, and illustrates one of the



conundrums in using model sensitivity as a model cleaning criterion – an issue that is considered further in Section 5: “Model Cleaning”.

EM Component Data Errors

Data errors estimated for and assigned to the eight EM data components (in-phase and quadrature for four frequencies 912, 3,005, 11,962 and 24,510 Hz) play a central role in controlling the inversion process and on output models generated by the inversion. Tikhonov-type inversion, as used by the *aempy* software, aims to converge on resistivity model solutions that fit the observed data to within their data errors. If data errors for all data components are the same, the inversion will aim to fit all components equally well. However, lower (or higher) errors assigned to a particular data component, will provide a stronger (or weaker) weighting towards fitting that component in the inversion. Assignment of data errors can therefore focus the inversion on different regions of the subsurface: for example, lower errors assigned to higher frequency data will tend to weight the inversion towards resolving shallower resistivity structure, and *vice versa* for lower errors assigned to lower frequency data and deeper structure. The *aempy* software allows data errors for all eight EM components to be assigned individually and separately.

Data errors for Block A5 were assessed using a statistical analysis of the data recorded in high-fly zones across the block (where particularly high flight clearances were required for operational reasons, e.g., over livestock farms and urban centres). High-fly zones provide opportunity to assess system noise levels away from geological and cultural noise signals. In the analysis, it is assumed that geological and cultural noise signals are negligible and that all recorded signal variation is due to system noise. Signal variation (noise) is assessed statistically by taking the standard deviation of the data. Table 3.2 summarises the results of the noise analysis for Block A5, where standard deviation values are reported for each data component for several data subsets. Data subsets were derived using flight clearance thresholds of 200, 240, 280 and 300 m (retaining all data above these thresholds). Between 200 and 280 m, standard deviations in all components are seen to decrease, suggesting that some residual geological or cultural noise signal may still be present in the data below 280 m. An estimate of the data errors



for each component was, therefore, derived using only the 280 and 300 m threshold data, taking the minimum standard deviation of the two (as summarised in the final row in Table 3.2, and tabled as Error-set 4 in Table 3.3).

Table 3.2: Data errors for A5 Block based on analysis of high-fly data. Subsets of the data were established using flight clearance thresholds of 200, 240, 280 and 300 m (retaining all data above these thresholds). The means and standard deviations of each data component were determined for each clearance subset. Percentage of data in each subset (column 2) is computed with respect to the 4,103,489 total number of data for A5 Block. Both traverse and tie-lines are included in the analysis. A5 delivery dataset used for the analysis is [GSI__18.IRL_DL2123_FEM.xyz]. Data in the bottom row of the table (minimum of the 280 and 300 m clearance subsets) are taken as estimates of the data errors for each component and tabled as Error-set 4 in Table 3.3.

Clearance threshold	Number and % of data		P09lev	P3lev	P12lev	P25lev	Q09lev	Q3lev	Q12lev	Q25lev
Clearance > 200 m	319,513	Mean (ppm)	67.2	165.4	308.0	139.4	49.0	201.6	289.3	308.4
	7.79%	SD (ppm)	56.7	68.4	90.4	132.6	58.0	67.0	81.0	103.8
Clearance > 240 m	208,507	Mean (ppm)	65.0	161.5	306.5	134.1	41.5	196.0	285.3	304.1
	5.08%	SD (ppm)	54.2	66.8	84.5	124.5	55.7	59.7	73.5	93.7
Clearance > 280 m	119,453	Mean (ppm)	63.0	158.9	306.0	129.2	34.6	193.3	286.9	303.2
	2.91%	SD (ppm)	54.0	65.4	79.4	116.8	55.0	53.6	69.3	90.0
Clearance > 300 m	66,055	Mean (ppm)	69.1	166.7	305.7	119.3	39.0	198.0	285.1	304.1
	1.61%	SD (ppm)	55.4	66.7	80.3	118.7	54.0	52.2	70.8	90.7
MINIMUM of >280m and >300m		SD (ppm)	54.0	65.4	79.4	116.8	54.0	52.2	69.3	90.0

While the analysis above suggests that system noise levels increase with increasing frequency, it is known from assessment of the EM dataset as a whole that, at the lower flight clearances prevalent across most of the survey area, cultural noise levels are higher for the lower frequency data and lower for the higher frequency data. In other words, it is not clear that noise levels assessed at high clearance levels are relevant to the modelling of data recorded at lower flight heights where the dominant noise source is cultural. Five additional “error-sets” (Table 3.3) were therefore tested in inversions of Test Dataset A (as defined above, consisting of 25, approximately 14-km long, profiles with ~55,000 sites in total). The “unweighted” error-set (Error-set 0), with equal errors for all data components, does not preferentially weight any component. Error-sets 1 and 2 (“hypothetical” error-sets) have lower errors for the higher frequency data components. Error-set 3 is derived from a similar statistical analysis to that carried out for Block A5 (using data standard deviations), in this case using the 240 m clearance data



flown in 2015 across the onshore portion of the Tellus Bundoran test line (source: Kiyani *et al.*, in review). In Error-set 3, the lowest data errors are found in the 3 kHz in-phase and quadrature components and the 25 kHz quadrature component. Error-set 5 is a modified version of Error-set 4 (derived in the analysis of Table 3.2 as discussed above), in which moderately lower errors are assigned to the two 25 kHz components – in response to test results indicating a degradation of model resolution in the shallowest parts of the model when using Error-set 4.

Table 3.3: Summary of Error-sets assessed by inversions of the 25 lines of Test Dataset A. Test numbers in the “comment” column correspond with Table 3.1.

Error-set	Errors (ppm)								Comment
	P09lev	P3lev	P12lev	P25lev	Q09lev	Q3lev	Q12lev	Q25lev	
0	60.0	60.0	60.0	60.0	60.0	60.0	60.0	60.0	"Unweighted" error-set. Test 18.
1	70.0	70.0	50.0	50.0	70.0	70.0	50.0	50.0	Hypothetical error-set, lower high-frequency errors. Test 19.
2	70.0	60.0	50.0	40.0	70.0	60.0	50.0	40.0	Hypothetical error-set, errors decreasing with frequency. Test 20.
3	54.1	27.6	68.1	46.1	54.7	21.0	60.7	28.6	Bundoran test line 2015, onshore portion, 240 m clearance (source: Kiyani <i>et al.</i> , in review). Test 21.
4	54.0	65.4	79.4	116.8	54.0	52.2	69.3	90.0	A5 Block high-fly analysis, clearance > 280 m. (Table 3.2). Test 22.
5	54.0	65.4	79.4	100.0	54.0	52.2	69.3	70.0	A5 Block high-fly analysis - modified, with 25 kHz errors reduced. Test 23.

Inversion tests of the six different error-sets were run on Test Dataset A using the FRA (non-independent inversions) strategy and the following data and parameter settings: clearance data low-pass filtered (20-fiducial), EM data filtered with PCA (Npca3) filter, and regularisation parameters $\tau_0 = 0.01$ and $\tau_1 = 6.0$. Output models from the tests are assessed in the sections below: (i.) qualitatively, examining resolution and depths of investigation in the models and (ii.) quantitatively by examining the data misfit residuals (in ppm) for all eight EM data components, where:

$$\text{misfit residual} = \text{predicted model response} - \text{observed response} \quad (5)$$

The observed responses in Equation 5 are the Npca3 filtered EM responses.



Misfit residuals (and their absolute values) are a more useful metric for test comparison purposes than RMS error. Misfit residuals reflect absolute differences between the predicted and observed responses (separately for each of the eight data components) and are “signed” (positive where the predicted responses are higher than the observed, and negative where lower). Model RMS errors reflect a misfit dependent on the data errors themselves (as the residuals are normalised by the data error in computing RMS error), are not “signed” (as the residuals are squared), and in summing all eight data components’ residuals together, lose information about the fit of individual components.

Table 3.4 summarises the results of the error-set inversion tests, showing means of the residuals and means of the absolute values of the residuals for all eight EM components and for all 6 error-set tests. Means are calculated across the ~55,000 sites and models in Test Dataset A. Results of Table 3.4 are shown graphically in Figures 3.14 and 3.15.

Table 3.4: Means of residuals and means of absolute values of residuals for all eight EM components and for 6 error-set tests. Means are calculated across the ~55,000 sites and models in Test Dataset A. In the case of absolute value data, a mean across all eight data components is computed, providing an overall measurement of the quality of fit for each error-set. Negative residual values are highlighted in red (where amplitude of predicted response is lower than observed response).

Inversion Test and Error-set	Eight Components Mean (ppm)	P09 Mean (ppm)	P3 Mean (ppm)	P12 Mean (ppm)	P25 Mean (ppm)	Q09 Mean (ppm)	Q3 Mean (ppm)	Q12 Mean (ppm)	Q25 Mean (ppm)
Absolute values of residuals									
18. Error-set 0	79.2	47.3	40.9	114.5	158.2	56.6	39.5	142.7	33.8
19. Error-set 1	80.6	53.1	48.9	104.9	157.4	61.1	45.9	142.8	31.0
20. Error-set 2	80.5	53.4	49.8	116.3	133.0	63.0	45.2	156.7	26.7
21. Error-set 3	78.9	55.0	32.5	139.5	137.0	59.6	23.6	162.5	21.1
22. Error-set 4	80.3	38.3	39.4	82.3	246.2	52.8	32.1	100.2	51.3
23. Error-set 5	79.1	40.1	40.0	97.0	216.1	52.8	32.9	116.2	37.4
Residuals									
18. Error-set 0		-29.3	11.5	-112.3	158.2	17.1	-2.8	-140.1	-2.2
19. Error-set 1		-36.0	13.0	-102.1	157.2	20.5	7.9	-140.4	-0.6
20. Error-set 2		-34.3	17.3	-113.0	133.0	21.5	4.5	-153.8	-1.3
21. Error-set 3		-24.2	19.3	-123.4	136.4	18.6	-8.6	-155.5	-6.4
22. Error-set 4		-18.6	14.2	-77.2	246.2	18.3	2.5	-95.9	15.3
23. Error-set 5		-21.0	12.2	-92.6	216.0	16.8	-2.7	-111.7	6.2



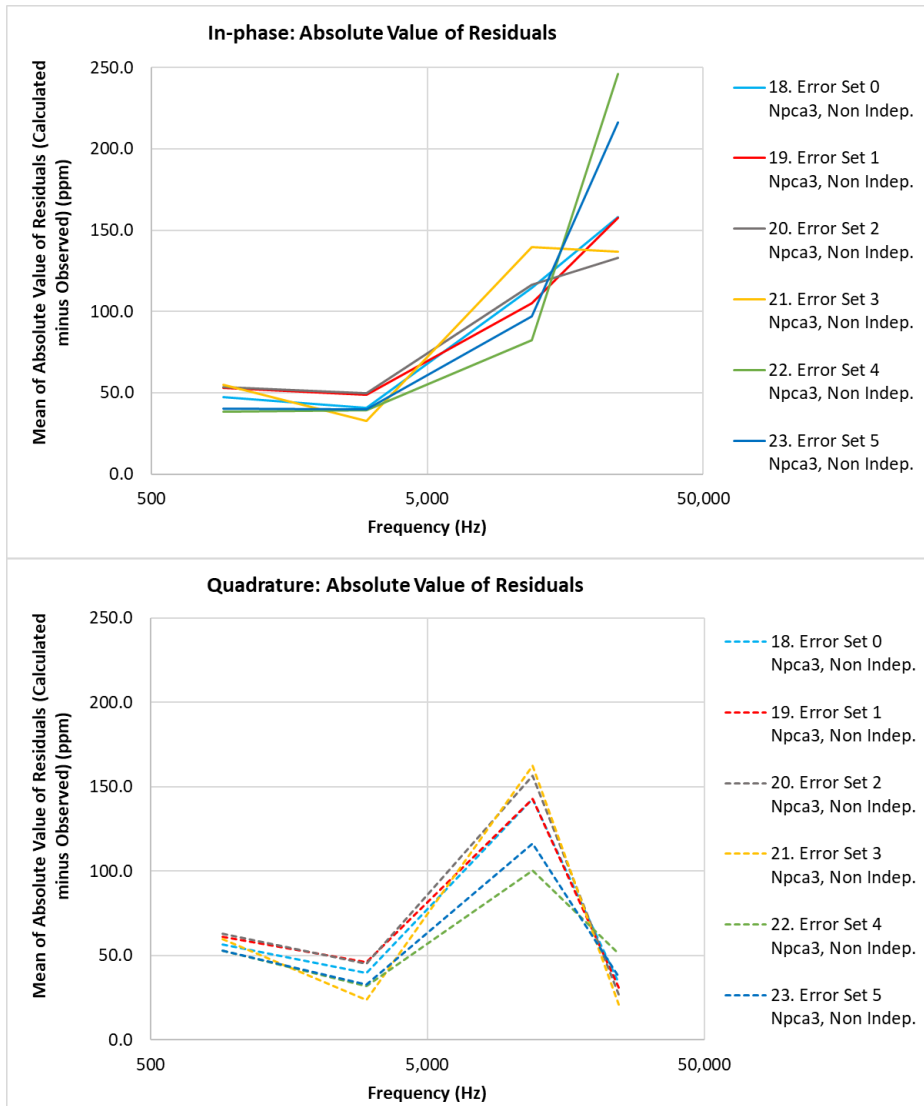


Figure 3.14: Data error test results (using Test Dataset A): Mean of the absolute values of residuals plotted for all 4 frequencies for (top) in-phase and (bottom) quadrature components. Error-set numbers (Table 3.2) and Test numbers (Table 3.1) are shown in the legend. Means are calculated for the ~55,000 sites in Test Dataset A.

An examination of the means of the absolute values of the residuals for each data component (Figure 3.14) shows similar trends regardless of the data error-set applied: both data components at 0.9 and 3 kHz, and quadrature at 25 kHz quadrature are well fit; in-phase and quadrature at 12 kHz are less well fit, and in-phase at 25 kHz is the poorest fit (with one exception, Error-set 3, Test 21). A notable feature in the residuals is the apparent trade-off between the fitting of the 12 and 25 kHz responses - most prominent in the in-phase data, but more subdued in the quadrature data. Where the fit at one frequency is enhanced through assignment of a lower data error, it is at the expense of a poorer fit for the other frequency. The trade-off is exemplified by two



tests: Test 22, Error-set 4 (lower error for in-phase 12 kHz improves 12 Hz fit but worsens the in-phase 25 kHz fit) and Test 21, Error-set 3 (lower error for in-phase 25 kHz improves 25 Hz fit but worsens the in-phase 12 kHz fit).

Averages of the eight component means of the residual absolute values (Table 3.4) provide a measurement of the overall quality of fit for each error-set test. These averages indicate a very similar overall quality of fit for all error-sets, all in the range 78.9 – 80.6 ppm, and further indicate that changing the relative sizes of data error between components (and therefore changing the relative weighting of the components in the inversion) redistributes the misfits between the components, without affecting the overall quality of fit for the entire dataset.

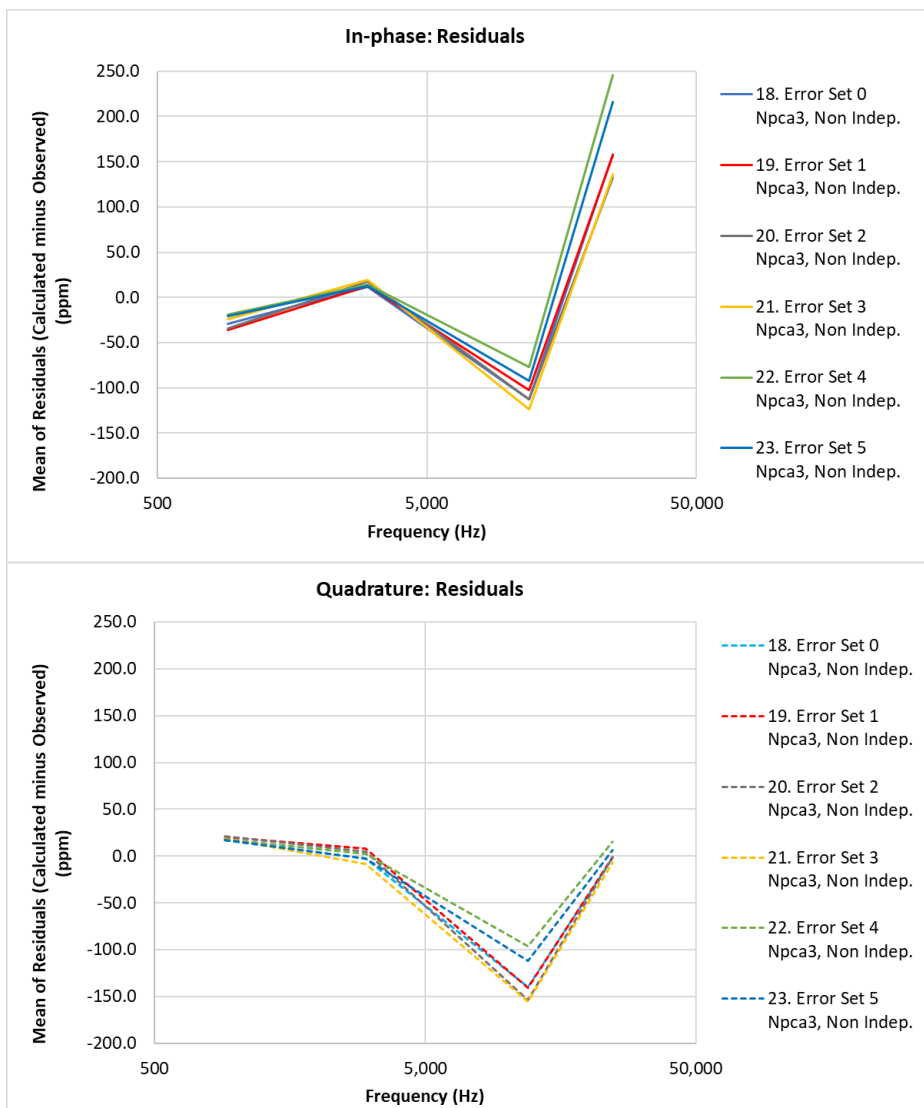


Figure 3.15: Data error test results (using Test Dataset A): Mean of residuals plotted for all 4 frequencies for (top) in-phase and (bottom) quadrature components. Error-set numbers (Table 3.2) and Test numbers (Table 3.1) are shown in the legend. Means are calculated for the ~55,000 sites in Test Dataset A.

Examining the means of the residuals for each data component (Figure 3.15) shows consistent mismatches, for all error-sets, between the predicted and observed data “baselines” for the in-phase components at 12 and 25 kHz and the quadrature component at 12 kHz. Predicted in-phase 12 kHz responses are on average around 90 ppm lower than the observed responses, predicted in-phase 25 kHz responses on average around 175 ppm higher, and predicted quadrature 12 kHz responses on average around 120 ppm lower. It is clear that the inversion resistivity models are unable to match simultaneously the average baselines in the observed data for these three data components. The trade-off between the 12 and 25 kHz frequencies, observed in the residual absolute value data and discussed above, in which a better fit at one frequency is achieved at the expense of the other frequency, is also apparent in the graphs of Figure 3.15.

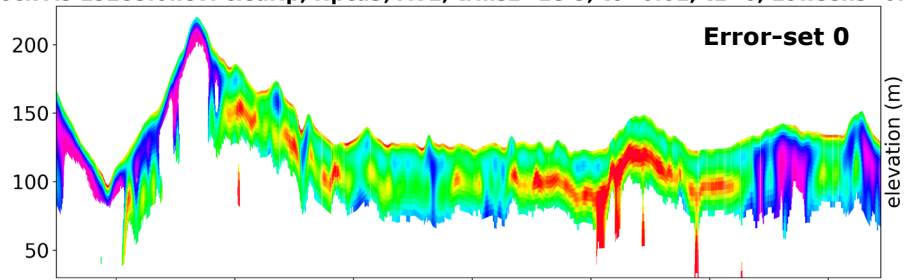
Further consideration of possible imbalances between the baselines of the observed 12 and 25 kHz data is beyond the scope of this current inversion work and report. However, the issue is one that merits further examination together with contractor SGL, possibly more usefully once a number of Tellus Blocks have been fully inverted.

Impacts on the output resistivity models of the different error-sets used are assessed in Figure 3.16. A general trend apparent in the models is that where higher frequencies are preferentially weighted (with lower data errors), there is some enhancement in the strength and continuity of the mid-level conductor at ~25 m depth, while at the same time some loss of sensitivity to resistors and in particular to the resistor at ~50 m depth near the centre of the profile (see models for Error-sets 1, 2 and 3). Conversely, where lower frequencies are preferentially weighted with lower data errors (Error-sets 4 and 5), imaging of deeper resistive structures is enhanced, but with significant degradation of the surficial and mid-level conductors in the model.

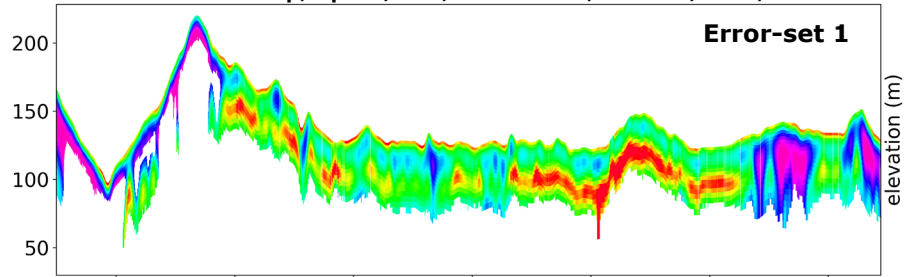
The unweighted errors of Error-set 0 (all errors = 60.0 ppm) are judged to provide a reasonable compromise between shallow and deep imaging in the models and have been adopted for the production inversion of Block A5.



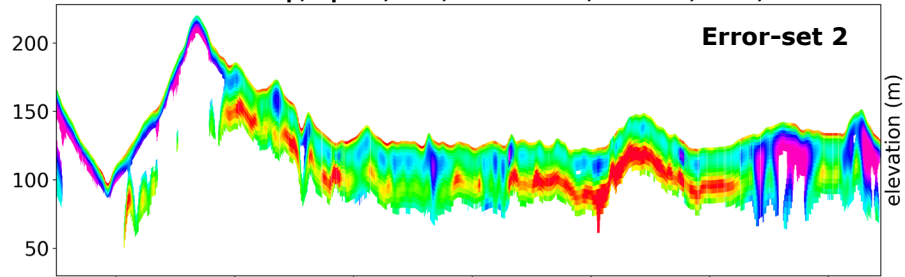
Block A5 L5285.0.lev: clearlp, Npca3, AVE, trms2=1e-5, t0=0.01, t1=6, Lowsens=0.0005



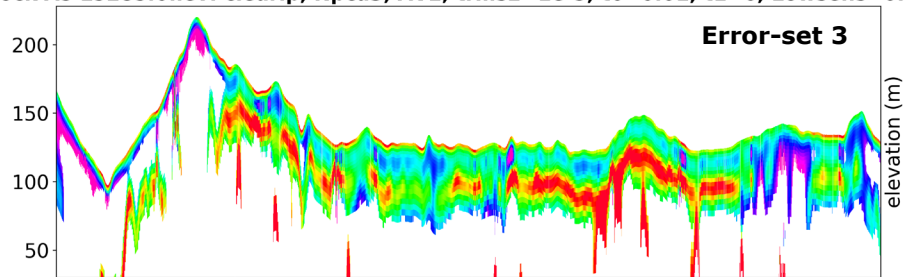
Block A5 L5285.0.lev: clearlp, Npca3, AVE, trms2=1e-5, t0=0.01, t1=6, Lowsens=0.0005



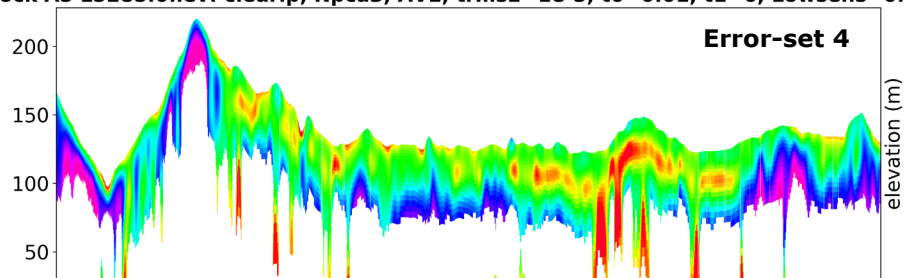
Block A5 L5285.0.lev: clearlp, Npca3, AVE, trms2=1e-5, t0=0.01, t1=6, Lowsens=0.0005



Block A5 L5285.0.lev: clearlp, Npca3, AVE, trms2=1e-5, t0=0.01, t1=6, Lowsens=0.0005



Block A5 L5285.0.lev: clearlp, Npca3, AVE, trms2=1e-5, t0=0.01, t1=6, Lowsens=0.0005



Block A5 L5285.0.lev: clearlp, Npca3, AVE, trms2=1e-5, t0=0.01, t1=6, Lowsens=0.0005

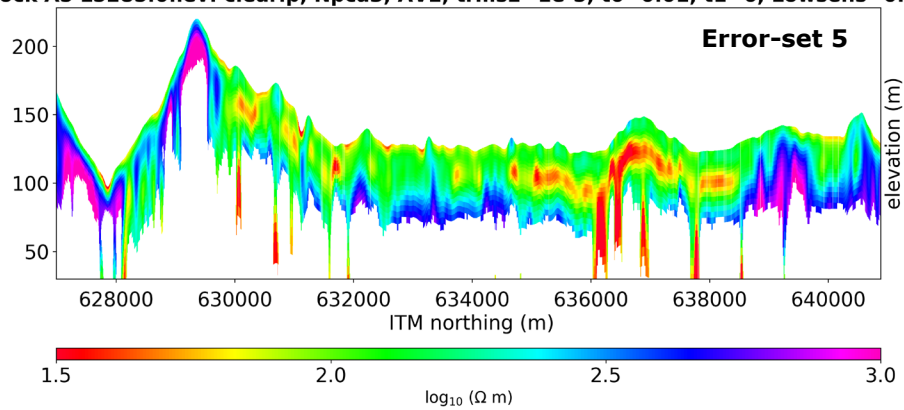


Figure 3.16: Line L5285 (Test Dataset A): Comparisons of output resistivity models for test inversions run using six different data error-sets (defined in Table 3.3). Model sections are presented in order from Error-set 0 at top to Error-set 5 at bottom. Models are blanked where normalised model sensitivity is less than a defined threshold of 0.0005 (the normalisation factor used is the maximum sensitivity for the profile, determined separately for each profile). North is to the right-hand side of the profiles.



4. Data Inversion

Inversion Parameters

Guided by the inversion tests reported on in Section 3, Tikhonov-type 1-D inversions were run on the full A5 Block dataset, on a line-by-line basis, using non-independent inversions coupled with the forward-reverse-average (FRA) strategy, in which models are computed in forward and reverse directions along each line and subsequently averaged. Inversion parameters and workflow are summarised in Table 4.1. Logarithmically increasing layer depths for the 35 layers used in the inversion are specified in Table 4.2.

The *aempy* software was run on two Windows 10 laptop computers, running *Python* (using the *Spyder* Integrated Development Environment) under *Ubuntu Linux* within an *Oracle VM VirtualBox*: (Laptop No. 1) Intel i7-8850H CPU @ 2.60 GHz, 32 GB RAM (with 16 GB virtual memory allocated to the virtual machine); and (Laptop No. 2) Intel i7-8750H CPU @ 2.20 GHz, 16 GB RAM (with 8 GB virtual memory allocated to the virtual machine).

A summary of several inversion statistics are reported below:

- i. Number of lines inverted: 525 (traverse lines only, no tie-lines inverted).
- ii. Total number of sites inverted: 3,725,100.
- iii. Inversion time: 302 runtime hours (~67% of sites inverted on Laptop No. 1 above, and ~33% inverted on Laptop No. 2).

Table 4.1. Inversion parameters and workflow. Amongst the data channels imported into *aempy* are: “MSLHGT” is the aircraft GPS Z coordinate and “PLM_nT” is the power line monitor (the latter imported into *aempy*, but not used).

PROCESSING STEP	SOFTWARE	PARAMETERS AND COMMENTS
Pre-processing		
Data import	<i>Geosoft</i>	Import into <i>Geosoft</i> . Input data file: [GSI__18.IRL_DLV2123_FEM.xyz]
Smoothing of laser altimeter data	<i>Geosoft</i>	Low-pass filter, 20-fiducial.



Data export	Geosoft	Export data channels required by <i>aempy</i> : line name, ITM_X, ITM_Y, MSLHGT, clearance_lp20, In-phase 0.9 to 25 kHz, Quadrature 0.9 - 25 kHz, PLM_nT.
Data import	<i>aempy</i>	Import into <i>aempy</i> software.
De-noising of EM data	<i>aempy</i>	Principal Component Analysis filter (Npca3 filter, retaining singular values 1, 2 and 3).
Tikhonov-type 1D regularised inversion		
Data inversion on a line-by-line, site-by-site basis	<i>aempy</i>	Number of layers (excluding final half-space): 35
		Layer thickness: increasing logarithmically, 2.0 m at surface to 9.6 m at 170 m depth.
		Starting model for first site on line: 100 ohm.m halfspace.
		Starting model for all other sites on line: previous site's 1-D model.
		Inversion direction on line: forward and reverse directions (i.e., two inversions per site).
		τ_0 regularisation parameter (closeness to starting model): 0.01
		τ_1 regularisation parameter (model smoothness): 6.0
		Data errors: 60.0 ppm for all 8 EM data components.
Model averaging	<i>aempy</i>	Compute average of forward and reverse direction runs: resistivity model, RMS errors, predicted EM responses and percentage difference between two models with respect to average model.
Data output	<i>aempy</i>	Output in <i>Geosoft</i> .XYZ format: resistivity model, model percentage difference, model sensitivity (all three sorted into depth channels), RMS error, predicted and observed EM responses.

Table 4.2. Model layer depths used in inversion of A5 Block EM data (depths recorded correspond with depth at the mid-point of the layer).

Depth Layer	D1	D2	D3	D4	D5	D6	D7	D8	D9
Depth (to mid-layer) (m)	1.0	3.0	5.2	7.4	9.8	12.3	14.9	17.6	20.5
Depth Layer	D10	D11	D12	D13	D14	D15	D16	D17	D18
Depth (to mid-layer) (m)	23.4	26.6	29.9	33.3	36.9	40.7	44.7	48.9	53.2
Depth Layer	D19	D20	D21	D22	D23	D24	D25	D26	D27



Depth (to mid-layer) (m)	57.8	62.6	67.7	72.9	78.5	84.3	90.4	96.7	103.4
Depth Layer	D28	D29	D30	D31	D32	D33	D34	D35	
Depth (to mid-layer) (m)	110.4	117.8	125.5	133.6	142.1	150.9	160.3	169.8	

Evaluation of Models and Fit

A range of different QC parameters are presented and considered here in assessing the reliability of the inversion models and their closeness of fit to the observed EM responses: site RMS error, misfit residuals, model percentage differences (between the forward and reverse line direction inversion models) and model sensitivity. Direct comparisons between observed and predicted EM response data are presented in Section 5 (“Model Cleaning”).

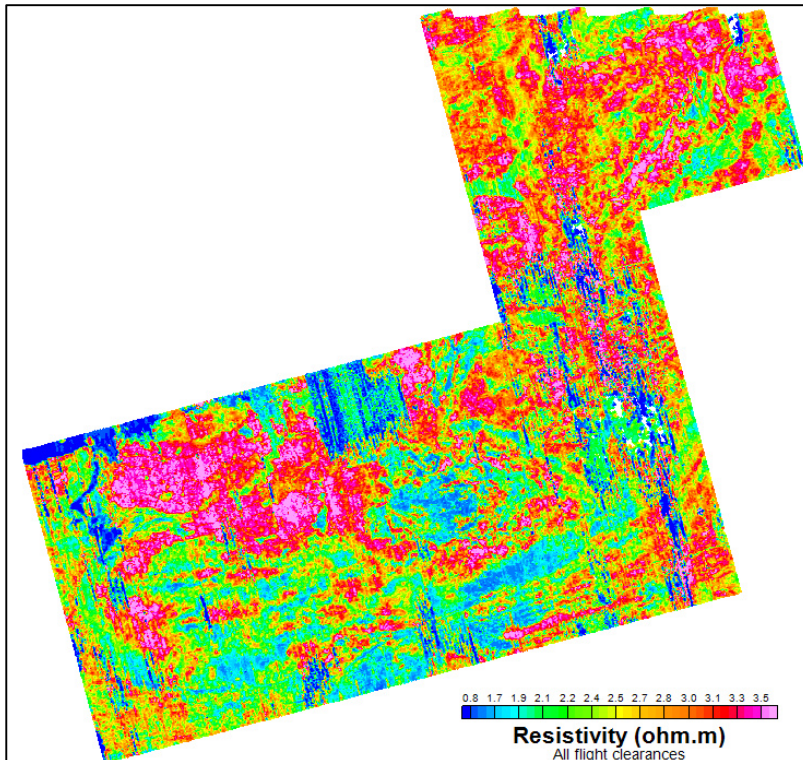
An example model output from the *aempy* inversions is shown in Figure 4.1, where the resistivity solutions for the 29.9 m depth layer are gridded and mapped across the survey area. A reassuring outcome of the modelling is that while the inversions were run independently on a line-by-line basis, there is nevertheless very good line-to-line continuity of geological features. Spatial resolution of the resistivity features also matches well the spatial variation observed in maps of the eight EM data components. High-fly areas are clearly recognised as anomalously high conductivity areas in the resistivity map, a result of the inversions returning (spurious) conductive bodies given, as input, very low EM component amplitudes and high flight heights.

RMS error provides a broad indication of the quality of the fit of the models to the observed data, with respect to the data errors. An RMS error equal to one indicates that the observed data are fit to within their data errors. Average RMS error statistics for the A5 Block inversion are as follows:

- **Mean RMS error = 1.805.** Standard Deviation = 1.873, total number of sites = 3,725,100.
- **Mean RMS error for clearance < 120 m = 1.516.** Standard Deviation = 1.835, total number of sites = 3,177,858 sites (85.3% of A5 total).



The lower mean RMS error calculated for sites with flight clearance < 120 m indicates that many of the poor model solutions are associated with high-fly areas – as further illustrated in Figure 4.2, where, in the lower figure, data with flight clearance > 120 m are blanked. In addition to high RMS errors associated with high-fly areas, there are also several individual lines, or portions of lines, and series of lines where RMS error is relatively high.



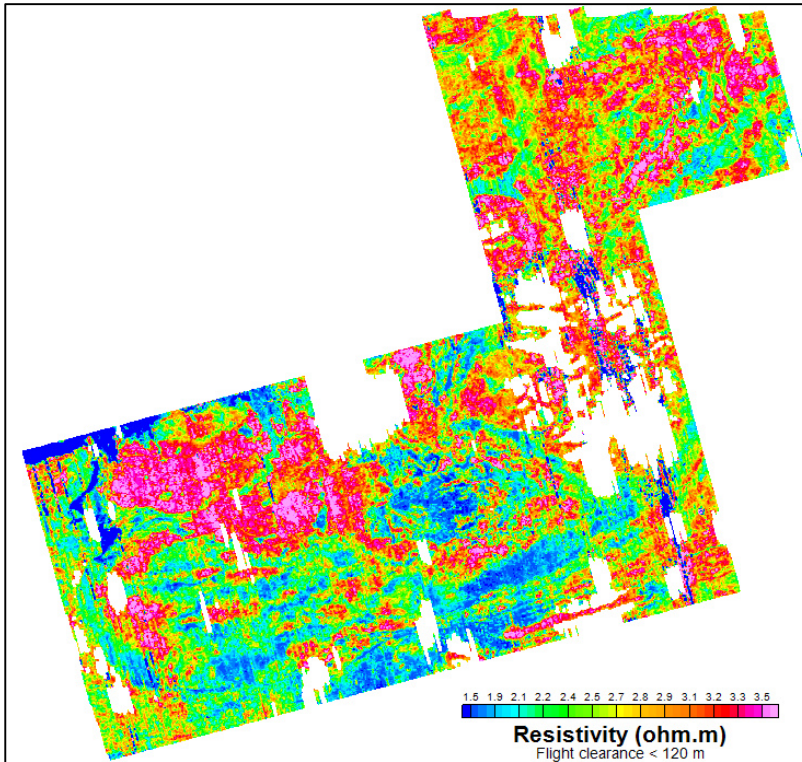
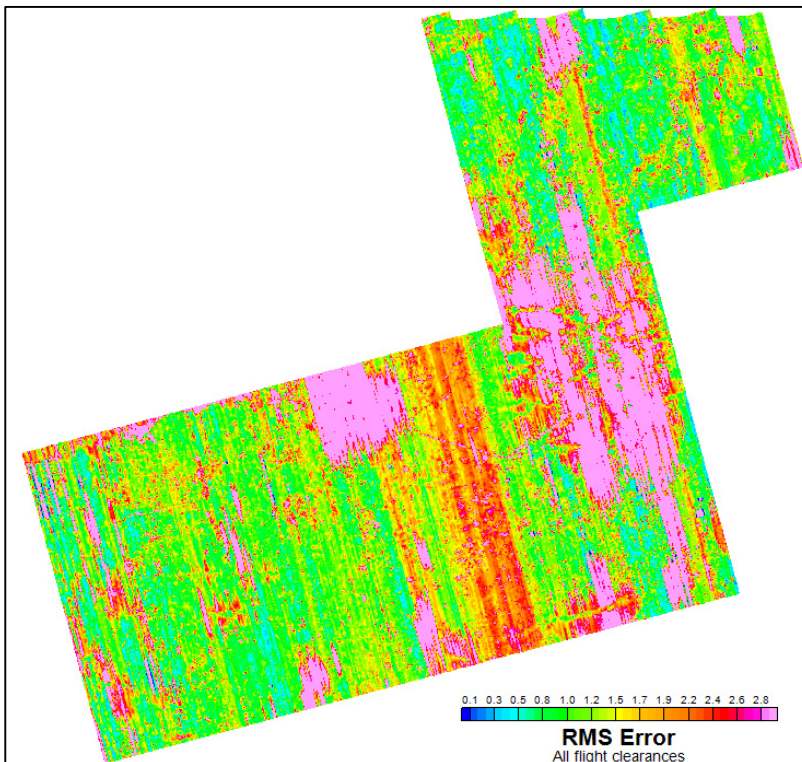


Figure 4.1: A5 Block EM inversion – grid maps of resistivity for the 29.9 m depth layer in the inversion models. (Top) full dataset. (Bottom) dataset blanked where flight clearance > 120 m. Grid mesh used is 50 x 50 m. The colour scale used has conductors shown in blue and resistors in red.



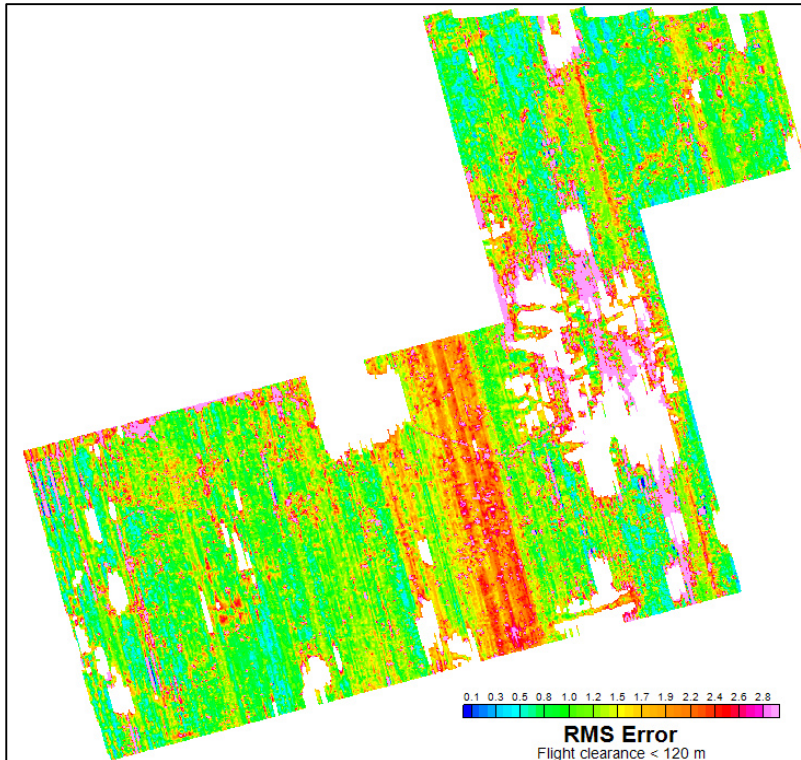


Figure 4.2: A5 Block inversion – grid maps of site RMS error. (Top) full dataset. (Bottom) dataset blanked where flight clearance > 120 m. Grid mesh used is 50 x 50 m.

Analysis of misfit residuals (Equation 5) for all eight EM data components, for both the full A5 dataset and the data subset where flight clearance < 120 m (Table 4.1 and Figure 4.3), indicates that the best fit EM components are in-phase and quadrature at 0.9 and 3 kHz. The worst fit component is in-phase at 25 kHz. While average misfits are high for both 12 kHz components for the full A5 dataset, they are much reduced when only considering the data subset with clearance < 120 m (the “low-fly” subset). Computing the average of the eight component means of the absolute value residuals (Table 4.1) provides a measurement of the overall quality of fit for the A5 inversion: 80.8 ppm for the full dataset and 67.0 ppm for the low-fly data subset. The latter figure is similar to the 60.0 ppm error assigned to the data, suggesting that the error assignment is of the right order.

The means of the residuals for the eight EM components reflect the same difficulty, as reported in the data error tests of Section 3, in matching the baselines of the observed 12 and 25 kHz data. In the low-fly data subset, the predicted in-phase responses for 12 and 25 kHz are on average 49.6 ppm lower and 112.9 ppm higher respectively than the observed responses. The predicted quadrature responses for 12 and 25 kHz are on average 69.4 ppm and 38.1 ppm lower respectively.



Table 4.1: A5 Block inversion misfit residuals: Means of residuals and means of absolute values of residuals for all eight EM components. Data presented for full dataset and dataset where clearance < 120 m. In the case of absolute value data, a mean across all eight data components is computed, providing an overall measurement of the quality of fit for the dataset. Negative residual values are highlighted in red (where amplitude of predicted response is lower than observed response). The total number of sites for the full A5 dataset is 3,725,100, and for the subset with clearance < 120 m, 3,177,858.

Dataset	Eight Components Mean (ppm)	P09 Mean (ppm)	P3 Mean (ppm)	P12 Mean (ppm)	P25 Mean (ppm)	Q09 Mean (ppm)	Q3 Mean (ppm)	Q12 Mean (ppm)	Q25 Mean (ppm)
Absolute values of residuals									
Full dataset	80.8	41.7	52.5	97.4	124.4	46.3	71.6	113.5	99.2
Clearance < 120 m	67.0	41.0	44.2	81.0	125.3	45.1	52.0	86.8	61.0
Residuals									
Full dataset		-4.3	-13.3	-70.2	93.9	6.0	-51.6	-98.6	-79.6
Clearance < 120 m		-4.7	-0.5	-49.6	112.9	13.3	-28.6	-69.4	-38.1

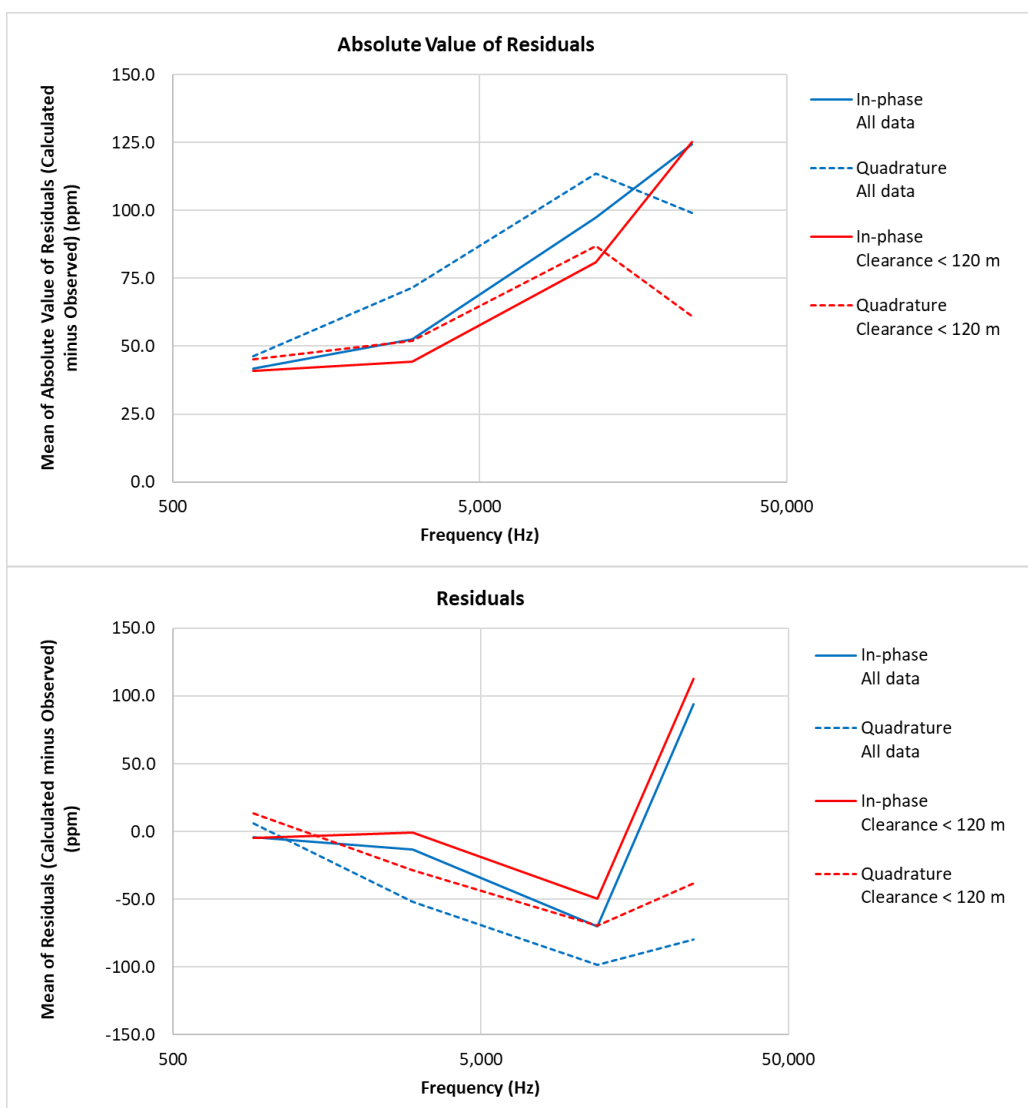
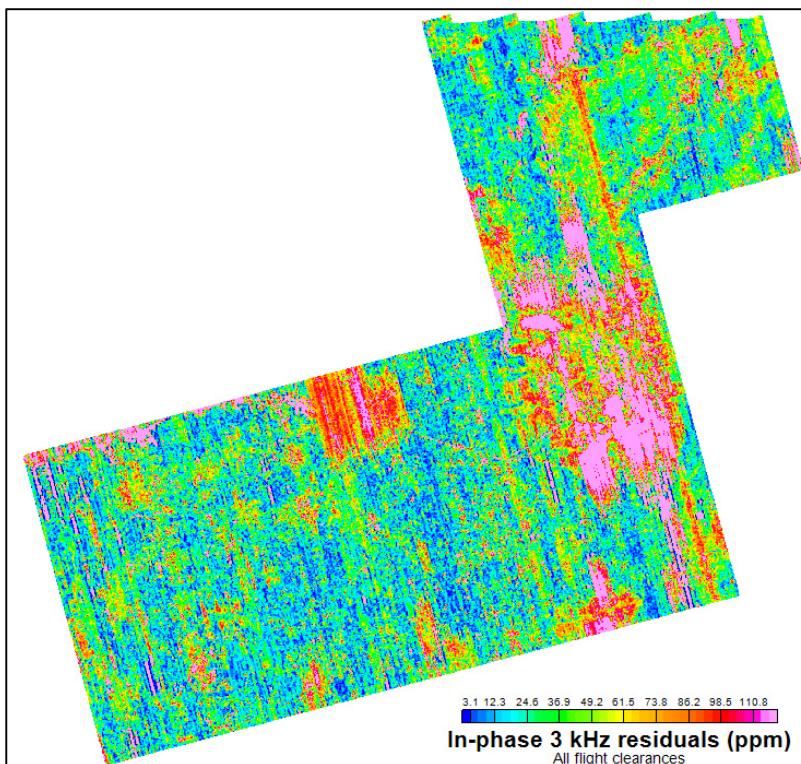


Figure 4.3: A5 Block inversion misfit residuals: (Top) Mean of absolute values of residuals plotted for all 4 frequencies for in-phase and quadrature components. (Bottom) Mean of residuals plotted for all 4 frequencies for in-phase and quadrature components. Analysis for all data shown (in blue) and for data where flight clearance < 120 m (in red).

The spatial distribution of misfit residuals, exemplified by that of the in-phase 3 kHz absolute value residuals (Figure 4.4), confirms a strong correlation between high residual values and high-fly areas. Blanking the residuals for flight clearances > 120 m (lower panel, Figure 4.4) removes most, but not all, of the high residual data in the vicinity high-fly zones. There are also several individual lines, or portions of lines where high residual values are apparent, as well as lineaments associated with power-line noise in the vicinity of Limerick City.



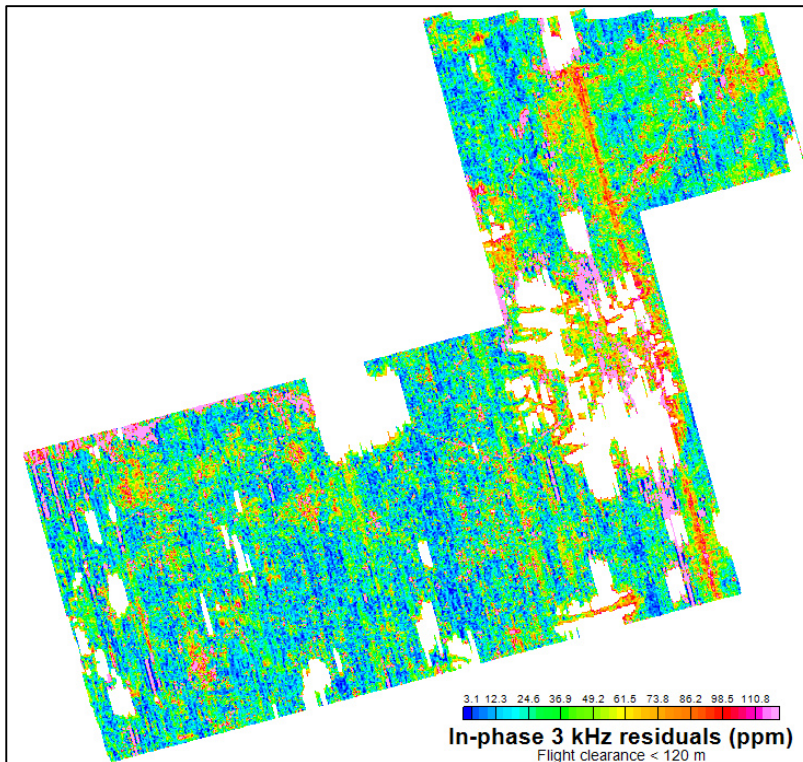


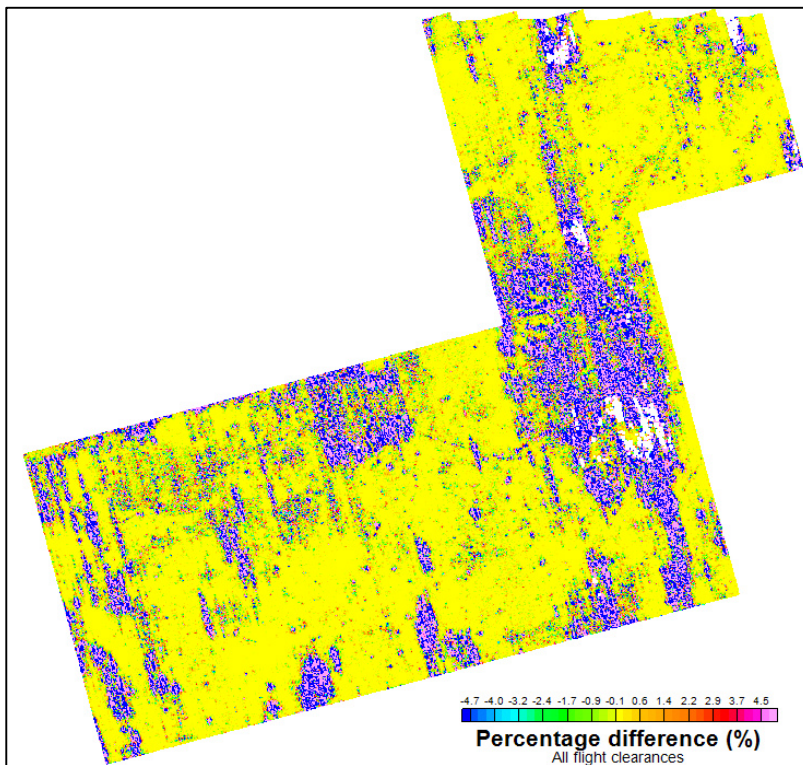
Figure 4.4: A5 Block inversion – grid maps of absolute values of misfit residuals for in-phase 3 kHz component (Top) full dataset. (Bottom) dataset blanked where flight clearance > 120 m. Grid mesh used is 50 x 50 m.

A further parameter from the inversion process that allows assessment of model quality and reliability is the percentage difference between the forward and reverse line direction inversion models. Similar to RMS error and misfit residuals, a strong spatial correlation is seen between large model percentage differences and high-fly areas – illustrated in Figure 4.5 for the case of the 29.9 m depth layer from the inversion models. Again, similarly, there are lines, or portions of lines where high percentage differences are apparent, as well as several clear lineaments associated with power-line noise in the vicinity of Limerick City.

A marked reduction in model sensitivity is apparent in high-fly areas, as illustrated in the example of the 29.9 m model depth layer in Figure 4.6. The model sensitivities have been normalised by the average sensitivity of the shallowest model layer, at 1.0 m depth, as explained further in Section 5. Conductive bodies in the subsurface are characterised by high sensitivities – hence the observed correlation between model sensitivity and geology.



There is a clear association between poor QC parameter responses and low model sensitivity, and high-fly areas and sources of cultural noise. Loss of geological signal strength with increasing flight clearance is dependent on the subsurface resistivity structure itself, with conductive and/or shallow bodies retaining signal strength to higher clearances than resistive and/or deeper ones. Using a universal flight clearance threshold as a model rejection criterion therefore runs the risk of rejecting reliable parts of the model if the clearance threshold is set too low, and retaining unreliable parts of the model if the threshold is set too high. Flight clearance rejection will also not address poor model solutions due to cultural noise in low-fly areas. Rather than using a broad-brush flight clearance threshold for model cleaning, a number of the QC parameters discussed in this section have been applied, with appropriate thresholds, to reject poor model solutions – as discussed in Section 5 below.



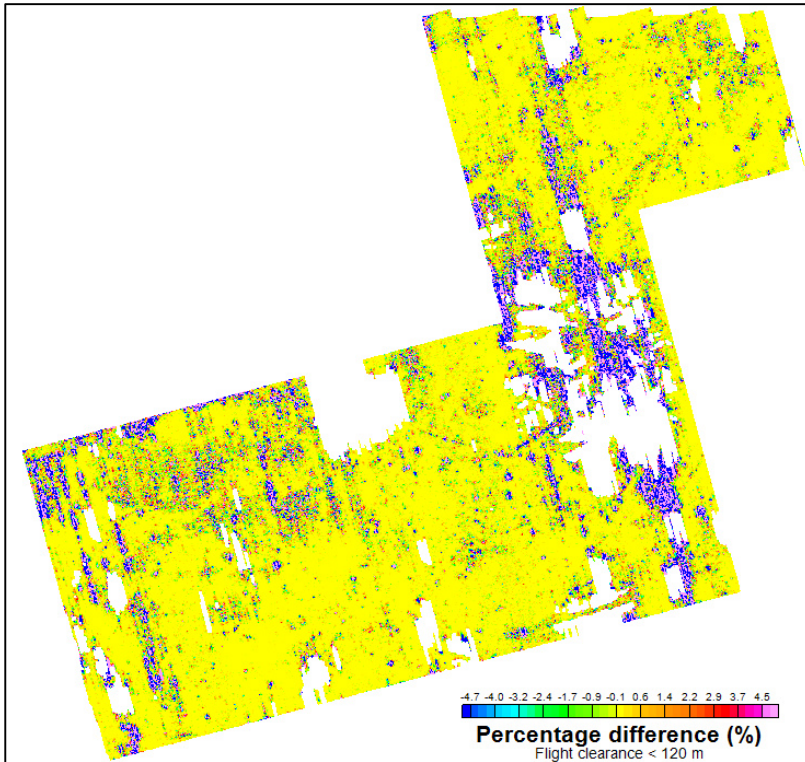
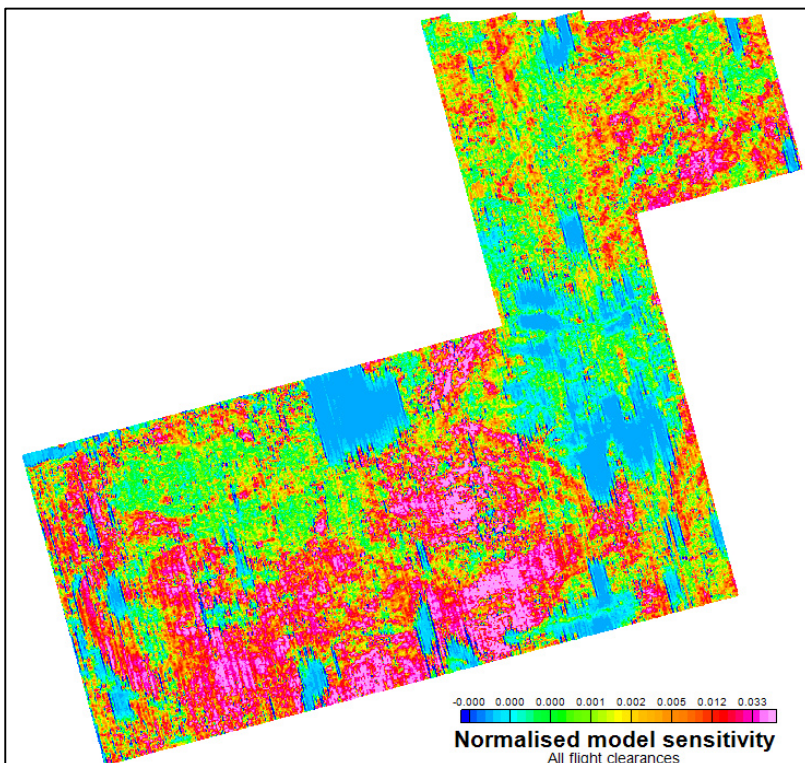


Figure 4.5: A5 Block inversion – grid maps of resistivity model percentage difference for 29.9 m depth layer (Top) full dataset. (Bottom) dataset blanked where flight clearance > 120 m. Grid mesh used is 50 x 50 m.



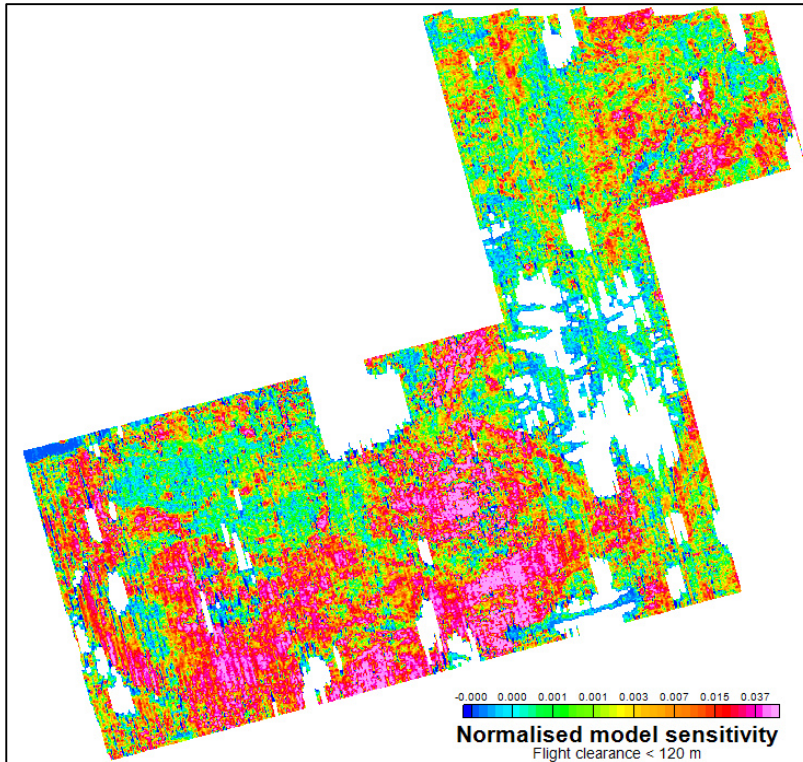


Figure 4.6: A5 Block inversion – grid maps of normalised model sensitivity for 29.9 m depth layer (Top) full dataset. (Bottom) dataset blanked where flight clearance > 120 m. Model sensitivities are normalised by the average sensitivity of the shallowest model layer, at 1.0 m depth, for the full dataset. Grid mesh used is 50 x 50 m.



5. Model Cleaning

The objective of “model cleaning” is to remove poor solutions from the models, primarily those associated with high-fly zones where geological signal strength is low, but also those resulting from cultural noise. Model cleaning was carried out within *Geosoft Oasis Montaj* software. Inversion resistivity models and supporting QC parameters, produced by *aempy*, were exported as ascii files in a format suitable for import into *Geosoft* (*Geosoft* .XYZ format). The model data for all sites remain in flight-line order, and resistivity values for each depth layer appear as separate resistivity channels when imported into a *Geosoft* database. Table 5.1 summarises the data channels exported from *aempy* and imported into *Geosoft*.

Table 5.1. List of data channels exported from *aempy* and imported into *Geosoft* software.

Data channels	Units	Description
LINE	-	Line number
ITM_X	m	X coordinate: IRENET95 ITM
ITM_Y	m	Y coordinate: IRENET95 ITM
DEM	m	Digital elevation model (referenced to sea level)
ALT	m	Flight clearance
P09npca3 to P25npca3	ppm	Observed in-phase 0.9 kHz to 25 kHz response (4 components, Npca3 filtered)
Q09npca3 to Q25npca3	ppm	Observed quadrature 0.9 kHz to 25 kHz response (4 components, Npca3 filtered)
P09calc to P25calc	ppm	Predicted in-phase 0.9 kHz to 25 kHz response (4 components)
Q09calc to Q25calc	ppm	Predicted quadrature 0.9 kHz to 25 kHz response (4 components)
RMSErr	-	Site RMS error
ResD1.0 to ResD169.8	log ₁₀ (ohm.m)	Model resistivity for 1.0 m depth layer to 169.8 m depth layer (35 depth layers)
QCpdiffD1.0 to QCpdiffD169.8	%	Model percentage difference for 1.0 m depth layer to 169.8 m depth layer (35 depth layers)
SensD1.0 to	ppm/ log ₁₀	Model sensitivity for 1.0 m depth layer to 169.8 m depth layer



SensD169.8	(ohm.m)	(35 depth layers)
------------	---------	-------------------

The model cleaning work flow is summarised in Table 5.2, together with the parameters and QC thresholds selected and used. The workflow was established by examination of the characteristics of different types of noise in the models and their correlations with the QC parameters derived from the *aempy* inversion. All operations were performed with resistivity values expressed as $\log_{10}(\text{resistivity})$. In the discussion that follows, for ease of expression, each depth layer is referred to in the form “Dn”, where *n* is the depth to the mid-point of the layer. For example, D1.0 and D29.9 refer to model layers at depths of 1.0 m and 29.9 m respectively. Thirty-four depth layers from D1.0 to D160.3 were processed through the initial two stages of the work flow, QC parameter threshold rejection, and smoothing and interpolation. Twenty-seven depth layers from D1.0 to D103.4 were passed on to the next stage, microlevelling, and subsequently the shallowest twenty depth layers to D62.6, assessed as robust and well constrained, were exported in several different data formats for public release.

Table 5.2. Model cleaning workflow and parameters. Depth layers are referred to in the form “Dn”, where *n* is the depth to the mid-point of the layer (e.g., D1.0 and D29.9 refer to model layers at depths of 1.0 m and 29.9 m respectively).

PROCESSING STEP	SOFTWARE	PARAMETERS AND COMMENTS
1. QC parameter threshold rejection (depth-by-depth, line-by-line basis)		
Normalise model sensitivity.	<i>Geosoft</i>	Normalise sensitivity (by division) using D1.0 whole-dataset average sensitivity = 242.859.
Apply normalised sensitivity (Nsens) threshold.	<i>Geosoft</i>	Apply only where flight clearance > 90 m. Reject model solution where sensitivity < sensitivity threshold. Depth dependent thresholds. For D1.0 to D9.8 = 0.01. For D12.3 to D26.6: variable, decreasing from 0.00871 to 0.00229. For D29.9 to D160.3 = 0.001.
Apply model percentage difference (QCpdiff) threshold.	<i>Geosoft</i>	Reject model solution where QCpdiff > 5% or QCpdiff < -5%.
Apply 3 kHz in-phase residual (P3resid) threshold.	<i>Geosoft</i>	Reject model solution where P3resid < -133.3 ppm or P3resid > 106.7 ppm (effectively a data mismatch greater than ± 120 ppm, allowing for mean residual for whole dataset of -13.3 ppm, Table 4.1).
2. Smoothing and Interpolation		
Smoothing of models on a line-by-line basis,	<i>Geosoft</i>	Low pass filter, 10-fiducial.



for each depth layer.		
Reject outlier model resistivities.	<i>Geosoft</i>	Reject model solution where $\log_{10}(\text{resistivity}) < -0.8$ or $\log_{10}(\text{resistivity}) > 4.0$. (For depth layer D1.0, rejects 0.05% of data at each end of the data distribution).
Interpolate models across short data gaps produced by data rejection, on a line-by-line basis, for each depth layer.	<i>Geosoft</i>	Akima interpolation, across maximum number of 2 adjacent missing data (i.e., across maximum 18 m gap).
3. Model microlevelling		
Grid all depth channels (layers).	<i>Geosoft</i>	Minimum Curvature algorithm, 50 x 50 m grid cell size.
Compute microlevelling-error grids, for each depth layer.	<i>Geosoft</i>	Butterworth high-pass filter (cut-off wavelength, λ , depth dependent: D1.0: $\lambda = 4000$ m, D3.1: $\lambda = 3200$ m, D5.2: $\lambda = 2600$ m, D7.5: $\lambda = 2000$ m, D9.8: $\lambda = 1600$ m, D12.3 - D103.4: $\lambda = 1200$ m) and Directional Cosine pass filter (azimuth 345°).
Resample microlevelling-error grids back to database and subtract from each depth layer.	<i>Geosoft</i>	
Convert $\log_{10}(\text{resistivity})$ values to resistivity values.	<i>Geosoft</i>	
Final gridding of microlevelled depth layers.	<i>Geosoft</i>	Inverse Distance Weighted (IDW) algorithm, 50 x 50 m grid cell size.

QC Parameter Threshold Rejection

The use of three different QC parameters was found both necessary and adequate to reliably remove poor or noisy model solutions from the dataset:

- i. **“Nsens”:** **normalised model sensitivity.** Absolute sensitivities (data channels SensD1.0 – SensD169.8 in Table 5.1) were normalised (divided) by a factor equal to the average sensitivity of the shallowest depth layer in the model (i.e., the average of SensD1.0), computed for the whole A5 Block. Normalised sensitivity data channels are then available for all depth layers (NsensD1.0 –



NsensD169.8). While absolute sensitivity could equally have been used for poor-model-solution rejection purposes, normalisation was performed with the aim of removing the effect, on sensitivity, of inversion specific parameters (e.g., data errors applied, EM data components active in the inversion, and number and thickness of model layers), so as to derive more “universally” applicable sensitivity and threshold values (for application to other model datasets derived using different inversion parameters, including inversions of further Tellus data blocks). Whether normalised sensitivity thresholds prove to be universally applicable remains to be tested, as further inversions on Tellus survey blocks are carried out in the future. One potential shortcoming in the strategy is, however, immediately apparent. As sensitivity is also dependent on the resistivity of the models, surveys across different geological terrains will encounter different shallow, overburden material, with different resistivity characteristics – i.e., the parameter used for normalisation – near-surface sensitivity – will not remain constant across large areas and different survey blocks.

It should be noted that the normalisation factor used here in Section 5 (and also in Section 4) is not the same as that used in the *aempy* model cross-sections presented in Section 3, where the normalisation factor is the maximum sensitivity for the whole model profile.

Application of the normalised sensitivity (*Nsens*) criterion is achieved in *Geosoft* using a conditional statement, where model solutions are rejected (nulled or dummied) where *Nsens* for that model solution is less than the specified threshold. Depth-dependent thresholds were defined to account for shallower layers naturally having greater sensitivities than deeper layers, with higher thresholds applied to shallower layers, and varying between 0.01 – 0.001 (Table 5.2). As resistive model layers are intrinsically associated with low sensitivities (see discussions above in previous sections), sensitivity threshold rejection was only applied for flight clearances greater than 90 m, in order to avoid the unnecessary rejection of resistive solutions in otherwise well resolved and constrained parts of the model.



- ii. **“QCpdiff”: model percentage difference.** *QCpdiff*, as discussed previously, is the percentage difference between the forward and reverse line direction inversion models, with respect to the average model. *QCpdiff* data channels are available for all depth layers (QCpdiffD1.0 – QCpdiffD169.8).

Application of the percentage difference (*QCpdiff*) criterion is achieved in *Geosoft* using a conditional statement, where model solutions are rejected (nulled or dummied) where *QCpdiff* for that model solution is greater than 5% or less than -5% (Table 5.2).

- iii. **“P3resid”: 3 kHz in-phase misfit residual.** The misfit residual for the in-phase 3 kHz data component is calculated as the predicted model response (P3calc in Table 5.1) minus the observed response (P3npca3). The 3 kHz in-phase misfit residual was preferred, in comparison with other component’s residuals, as a model-solution rejection criterion as it has low means for both the residuals and the absolute value residuals (Table 4.1), the former indicating a good fit for this component to the baseline of the observed data and the latter indicating generally good levels of fit to the observations. Lower cultural noise levels and stronger geological signal for this component make it preferable to the 0.9 kHz in-phase and quadrature residuals.

Application of the in-phase 3 kHz residual (*P3resid*) criterion is achieved in *Geosoft* using a conditional statement, where model solutions are rejected (nulled or dummied) where *P3resid* for that model solution is greater than 106.75 ppm or less than -133.3 ppm (Table 5.2). The asymmetry of the thresholds accounts for the mean of the in-phase 3 kHz residuals being offset from the observed data baseline by -13.3 ppm (Table 4.1).

The effect of high flight clearances on the EM responses and on the inversion model solutions is clearly visible when examining these data along flight lines (Figures 5.1 and 5.2). There is a sharp and recognisable lateral transition from EM responses containing meaningful geological signal, corresponding with laterally coherent inversion solutions, to very low amplitude EM signals with low to zero geological signal, corresponding with erratic and spurious model solutions. In the example of Figures 5.1 and 5.2, the transition occurs at a flight clearance of around 130.1 m, for all model depth solutions shown (1.0 m, 14.9 m and 29.9 m depth). It is not always the case that all depth layers



lose coherency at the same flight clearance – more often, shallower depth layers (or more conductive bodies) retain coherency to higher clearances than deeper layers (or more resistive bodies).

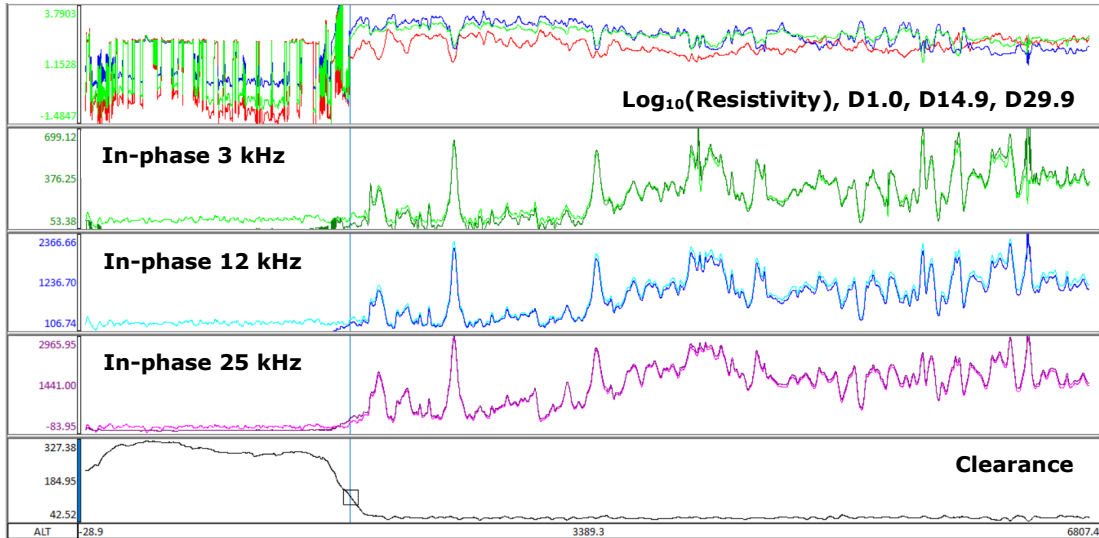


Figure 5.1: A5 Block inversion models and data fit, line L5189 (40.4 km line length). (Top) Resistivity profiles for model depth layers D1.0 (red), D14.9 (green) and D29.9 (blue). (Second from top) In-phase 3 kHz observed (light green) and predicted (dark green) responses. (Middle) In-phase 12 kHz observed (light blue) and predicted (dark blue) responses. (Second from bottom) In-phase 25 kHz observed (light violet) and predicted (dark violet) responses. (Bottom) Flight clearance (black). Cursor locality shows transition from good to poor model solutions, corresponding with flight clearance = 130.1 m.

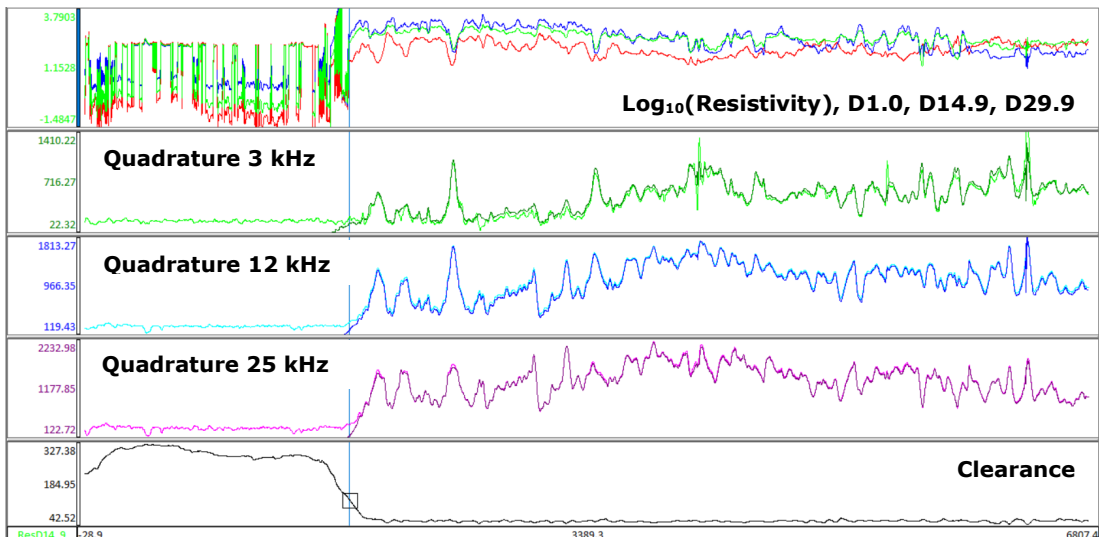


Figure 5.2: A5 Block inversion models and data fit, line L5189 (40.4 km line length). (Top) Resistivity profiles for model depth layers D1.0 (red), D14.9 (green) and D29.9 (blue). (Second from top) Quadrature 3 kHz observed (light green) and predicted (dark green) responses. (Middle) Quadrature 12 kHz observed (light blue) and predicted (dark blue) responses. (Second from bottom) Quadrature 25 kHz observed (light violet) and predicted (dark violet) responses.



(Bottom) Flight clearance (black). Cursor locality shows transition from good to poor model solutions, corresponding with flight clearance = 130.1 m.

The clear, visual expression of poor model solutions, when viewed as along-line resistivity profiles (cf., Figures 5.1 and 5.2), allowed appropriate threshold values for the three QC criteria to be determined empirically – through careful testing and visual assessment of a large number of flight lines and all depth layers – leading to the threshold values defined in Table 5.2 and applied to the full A5 model dataset using *Geosoft* scripts to automate the process.

The process of model-cleaning using thresholds defined for the three QC criteria, *Nsens*, *QCpdiff* and *P3resid*, is illustrated in Figures 5.3 and 5.4, for the case of model depth layer D1.0 along a short 10 km-long section of line L5005. The green resistivity profile in these figures shows the original model solutions, and the red resistivity profile the cleaned (or accepted) model solutions. Poor model solutions and poor fits to the observed data are associated with a high-fly zone in the middle of the line section. The cursor in Figure 5.4 shows the locality where normalised sensitivity (*NsensD1.0*) is just below the applied threshold value of 0.01, corresponding with a flight clearance of 164.1 m. There are visibly poor solutions to the left of the cursor, where sensitivity is higher than the threshold, that have not been rejected by the sensitivity criterion (*NsensD1.0* = 0.032 at the onset of the poor model solutions, where flight clearance = 147.5 m). However, these poor solutions (with sensitivities greater than the sensitivity threshold) have been rejected by both the *QCpdiff* and *P3resid* criteria. It is practically very difficult, within an automated model-cleaning scheme, to define widely applicable threshold values that will reject all poor model solutions under all circumstances, for all depths, flight clearances and model resistivities. The efficacy of the automated approach relies on the mutual support provided by the simultaneous use of three different criteria.



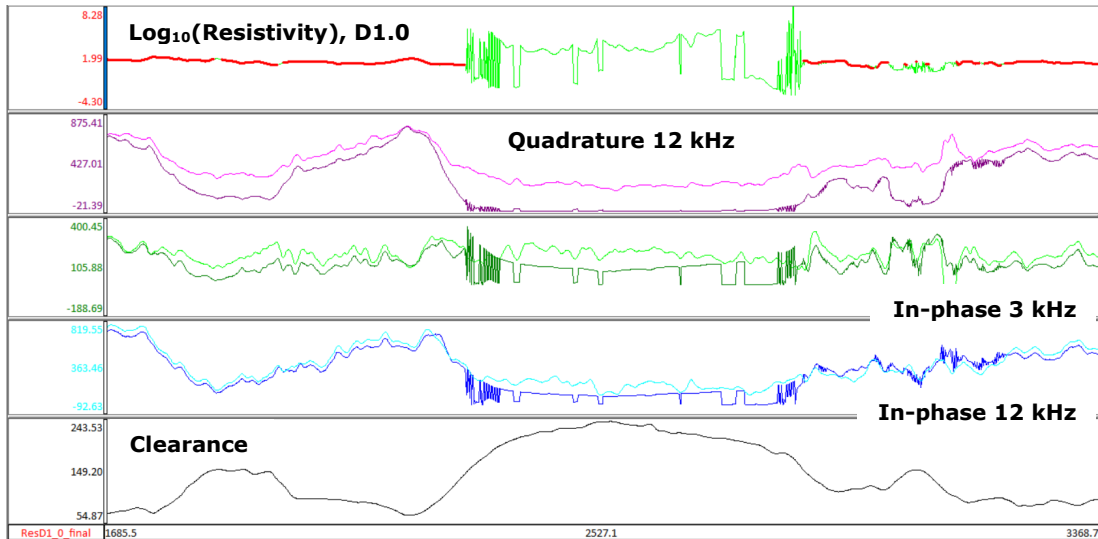


Figure 5.3: A5 Block inversion model and data fit, line L5005 (10.1 km-long line section). (Top) Resistivity profiles for model depth layer D1.0, original and uncorrected (green) and cleaned using QC criteria (red). (Second from top) Quadrature 12 kHz observed (light violet) and predicted (dark violet) responses. (Middle) In-phase 3 kHz observed (light green) and predicted (dark green) responses. (Second from bottom) In-phase 12 kHz observed (light blue) and predicted (dark blue) responses. (Bottom) Flight clearance (black).

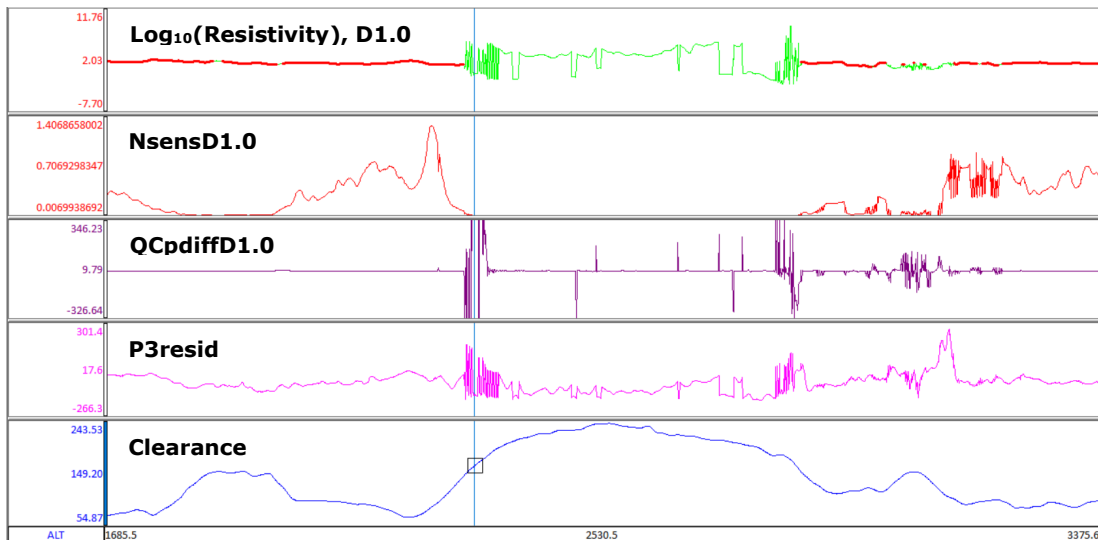


Figure 5.4: A5 Block inversion model and QC criteria, line L5005 (10.1 km-long line section). (Top) Resistivity profiles for model depth layer D1.0, original and uncorrected (green) and cleaned using QC criteria (red). (Second from top) Normalised sensitivity – NsensD1.0 QC parameter (red). (Middle) Model percentage difference – QCpdiffD1.0 QC parameter (dark purple). (Second from bottom) In-phase 3 kHz residual – P3resid QC parameter (violet). (Bottom) Flight clearance (blue). Cursor shows locality where NsensD1.0 value (0.0097) is less than the QC threshold = 0.01, corresponding with flight clearance = 164.1 m.



Smoothing, Outlier Resistivity Value Rejection and Interpolation

Away from high-fly areas and sources of cultural noise, resistivity values within each model depth layer generally show good lateral continuity and smooth variation from site to site (an outcome reinforced by the non-independent inversion strategy used). However, there are instances of low amplitude, site to site resistivity variations, where the inversion models appear to oscillate between moderately different preferred solutions from site to site. An example of the oscillating behaviour in the 29.9 m depth layer is shown in Figure 5.5, along a 1.7 km-long section of line L5489. The maximum amplitude of the resistivity oscillations is 87 Ω .m. While these oscillations are reflected in all three QC criteria, *NsensD29.9*, *QCpdiffD29.9* and *P3resid*, the QC thresholds are not exceeded and none of the model solutions are rejected.

Application of a 10-fiducial (~60 m wavelength) low-pass filter, on a line-by-line basis, was found to effectively remove the site-to-site resistivity oscillations, as well as isolated model spikes not caught by the QC rejection criteria, without altering the resistivity solutions away from problematic areas. **The 10-fiducial low-pass filter was applied to all depth layers in the dataset.**

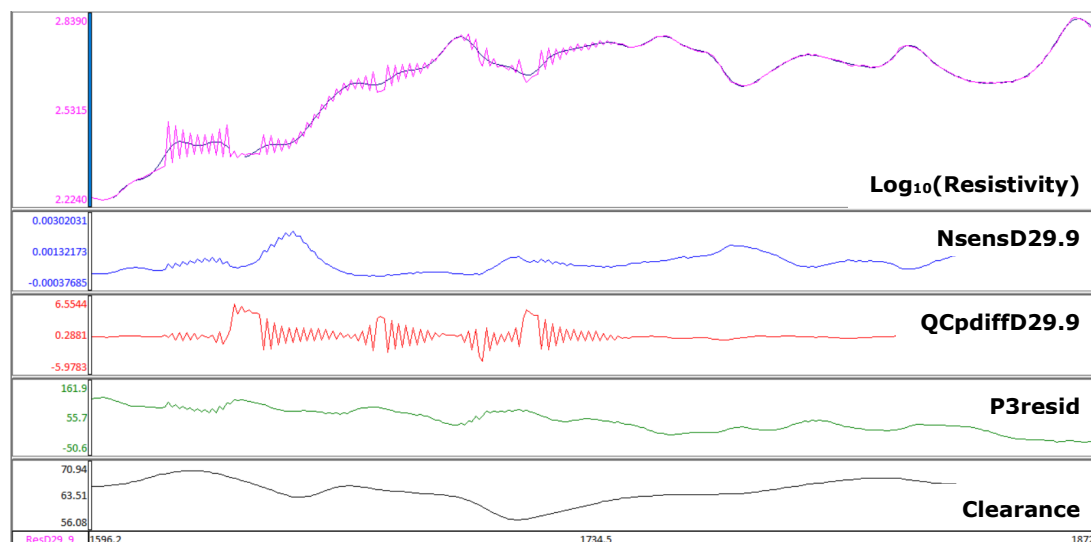


Figure 5.5: A5 Block inversion model and QC criteria, line L5489 (1.7 km-long line section). (Top) Resistivity profiles for model depth layer D29.9, original and uncorrected (violet) and low-pass filtered (10-fiducial) (blue). (Second from top) Normalised sensitivity – *NsensD29.9* QC parameter (blue). (Middle) Model percentage difference – *QCpdiffD29.9* QC parameter (red). (Second from bottom) In-phase 3 kHz residual – *P3resid* QC parameter (dark turquoise). (Bottom) Flight clearance (black).



In a small number of instances, extremely low or high resistivity values are returned in the inversion model solutions, and these extreme values are not always captured and rejected by the QC criteria. **Extreme values have therefore been rejected using the following criteria: reject solutions where $\log_{10}(\text{resistivity}) < -0.8$ (= 0.16 $\Omega\cdot\text{m}$) or $\log_{10}(\text{resistivity}) > 4.0$ (= 10,000 $\Omega\cdot\text{m}$).** For the D1.0 depth layer, these criteria reject 0.05% of the model solutions on each side of the resistivity data distribution.

The final model-cleaning process applied is that of interpolation, to fill in short gaps in the along-flight-line resistivity profiles resulting from very localised rejection of poor model solutions (e.g., spikes). **An Akima interpolation was applied on a line-by-line basis, for all depth layers, across a maximum number of 2 adjacent missing data points (i.e., across a maximum gap of 18 m).** The size of the gap filled by the interpolation is commensurate with the size of the EM imaging footprint on the ground and in the subsurface.

Gridded examples, for a number of representative depth layers (3.1 m, 12.3 m, 29.9 m and 62.6 m depths) taken from the final cleaned resistivity dataset, are provided in the section below.

Microlevelling of Resistivity Model Data

Although the EM response data used as input for the resistivity inversions are well levelled, relatively minor residual line-to-line variations in these data manifest themselves, amplified, as line-to-line variations in the resistivities of the inversion models. Line-to-line variations (or levelling errors) are particularly pronounced in the shallowest model layers above 10 m depth (e.g., Figure 5.6, showing resistivity grids for the 3.1 m depth layer). Microlevelling of the final, cleaned model dataset was carried out to remove line-to-line variations, treating each depth layer separately and following the workflow summarised in Table 5.2 and described in further detail below. The resistivity data for twenty-seven depth layers, from D1.0 to D103.4, were microlevelled. Further examples of the resistivity data grids, pre- and post-microlevelling, are shown in Figures 5.8, 5.9 and 5.10 for depth layers D12.3, D29.9 and D62.6 respectively.



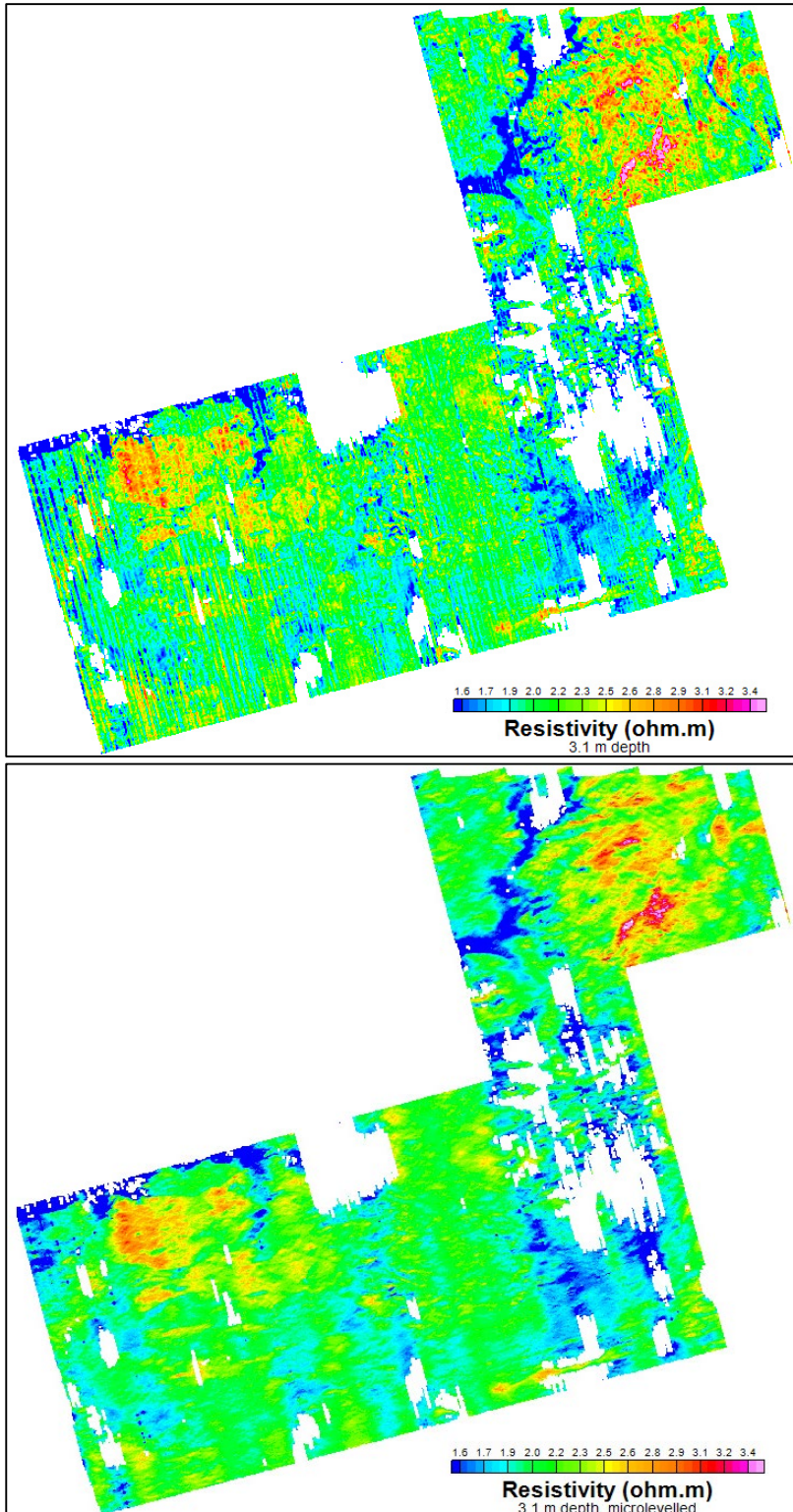


Figure 5.6: A5 Block EM inversion – grid maps of resistivity for 3.1 m depth layer. (Top) Final cleaned dataset. (Bottom) Final cleaned dataset after microlevelling. Models are blanked where solutions fall outside the threshold limits of the three QC criteria applied: NsensD3.1, QCpdiffD3.1 and P3resid. Minimum curvature gridding is used, with 50 x 50 m grid mesh.



Following gridding of the final, clean resistivities for all depth layers, the microlevelling procedure consists of computing microlevelling-error grids, in which line-to-line differences (errors) are isolated, by applying dual Butterworth high-pass and Directional Cosine filters to the final resistivity grids. The example microlevelling-error grid of Figure 5.7, for depth layer D3.1, illustrates the line-to-line differences extracted from the final D3.1 resistivity grid of Figure 5.6 (upper grid). Subtraction of the microlevelling-errors yields the final microlevelled D3.1 resistivity grid of Figure 5.6 (lower grid). Practically, the subtraction of microlevelling-errors is achieved by re-sampling the microlevelling-error grids back to the line database, as a new data channel, where they are subtracted from the resistivity data channels, to produce line-based, microlevelled resistivity data for each depth layer – the final product of the EM inversions. It is noted that microlevelling was carried out with resistivities in the \log_{10} domain. $\log_{10}(\text{resistivity})$ values are converted to resistivity values for the public release of the inversion models.

Depth-dependence was required in the specification of the cut-off wavelength of the Butterworth high-pass filter that was applied to isolate levelling errors from the resistivity model data (see specifications in Table 5.2). At shallower depths (D1.0 – D9.8), the resistivity data grids (pre-microlevelling) are characterised by longer wavelength levelling errors (in a direction perpendicular to the line direction), requiring longer cut-off wavelengths in the filter. Compared with the 1,200 m cut-off wavelength for depth layers D12.3 and greater, cut-off wavelengths increased from 1,600 m for D9.8 to 4,000 m for D1.0. Using the 1,200 m cut-off wavelength for the shallower depth layers resulted in undesirable broad bands of resistivity variation in the output microlevelled resistivity grids, running across the survey area, parallel to the line direction.



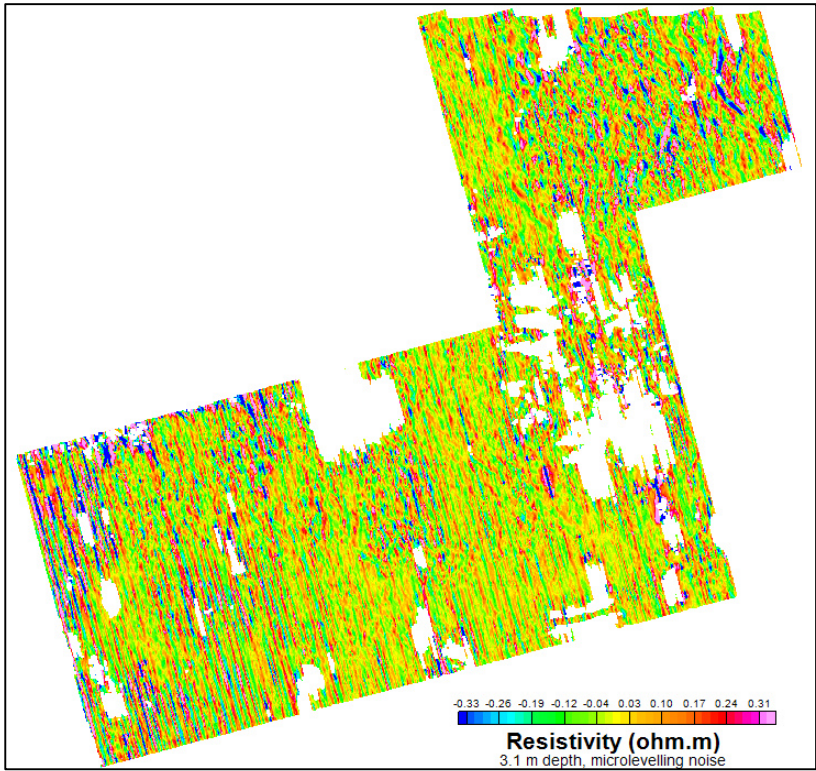
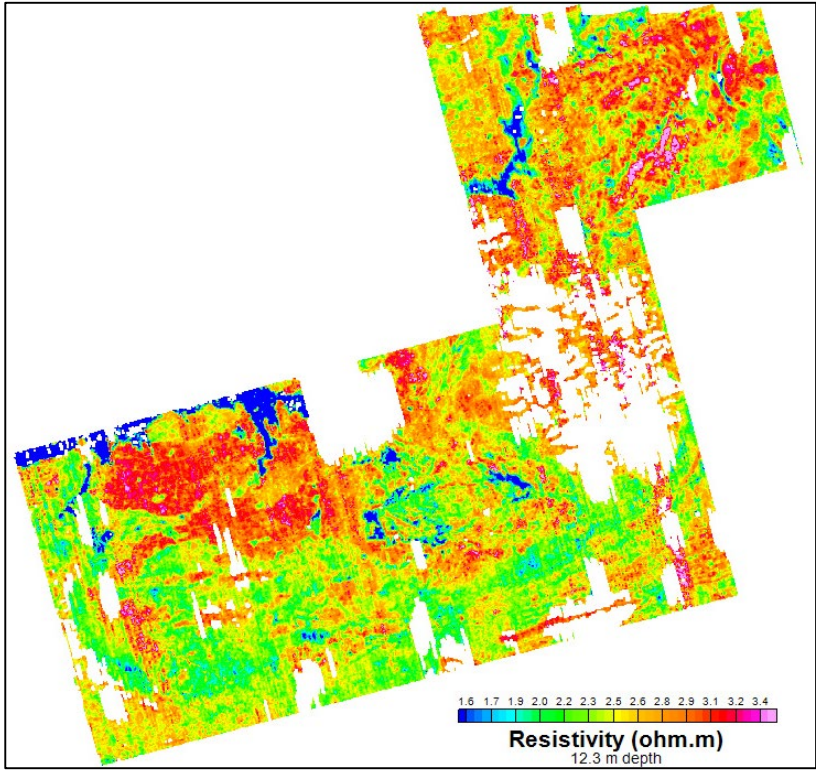


Figure 5.7: A5 Block EM inversion – grid map of microlevelling-error for 3.1 m depth layer. Models are blanked where original resistivity model solutions fall outside the threshold limits of the three QC criteria applied: NsensD3.1, QCpdiffD3.1 and P3resid. Minimum curvature gridding is used, with 50 x 50 m grid mesh.



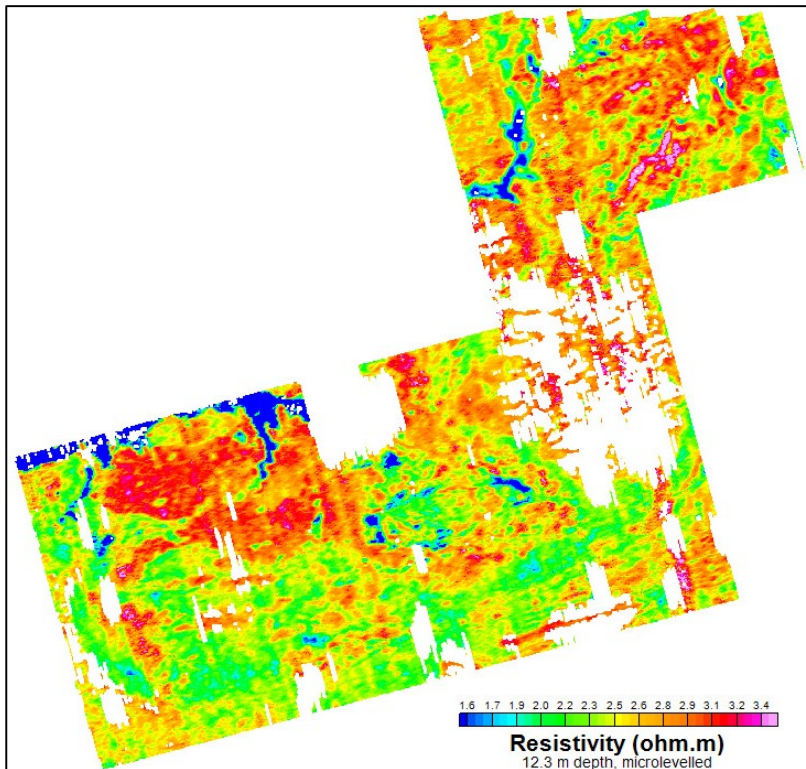
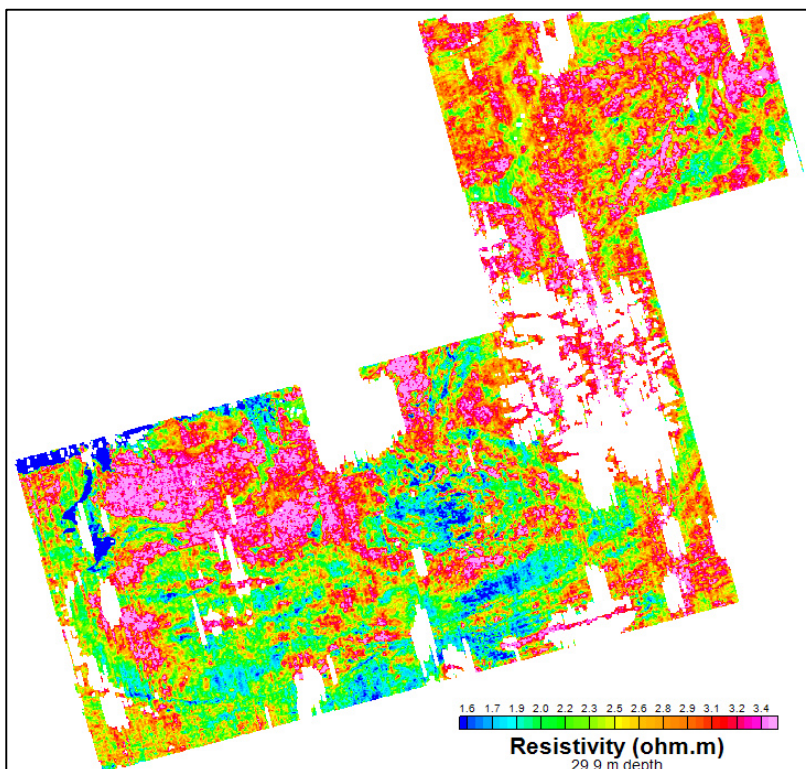


Figure 5.8: A5 Block EM inversion – grid maps of resistivity for 12.3 m depth layer. (Top) Final cleaned dataset. (Bottom) Final cleaned dataset after microlevelling. Models are blanked where solutions fall outside the threshold limits of the three QC criteria applied: NsensD12.3, QCpdiffD12.3 and P3resid. Minimum curvature gridding is used, with 50 x 50 m grid mesh.



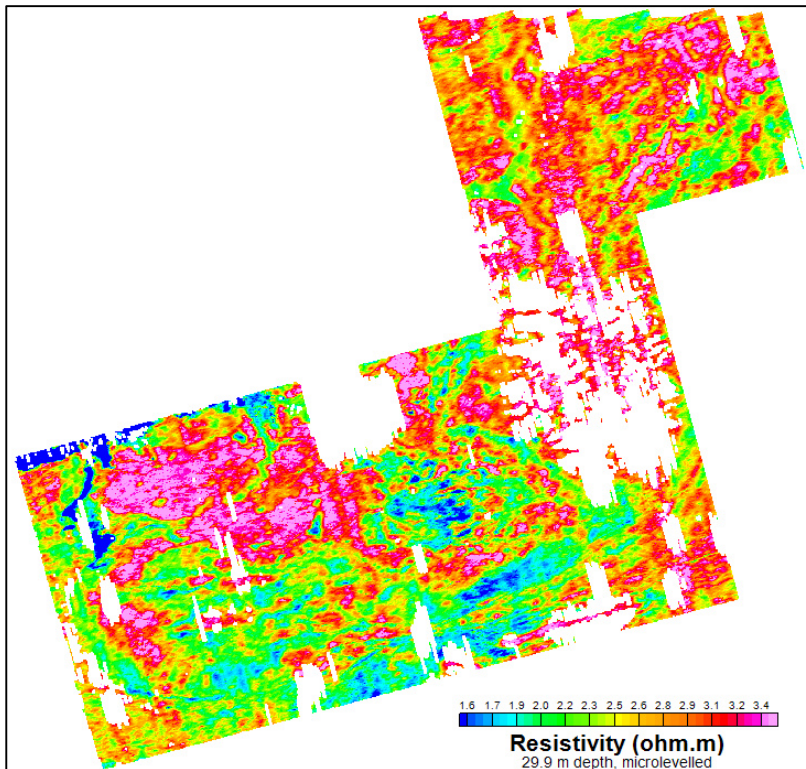
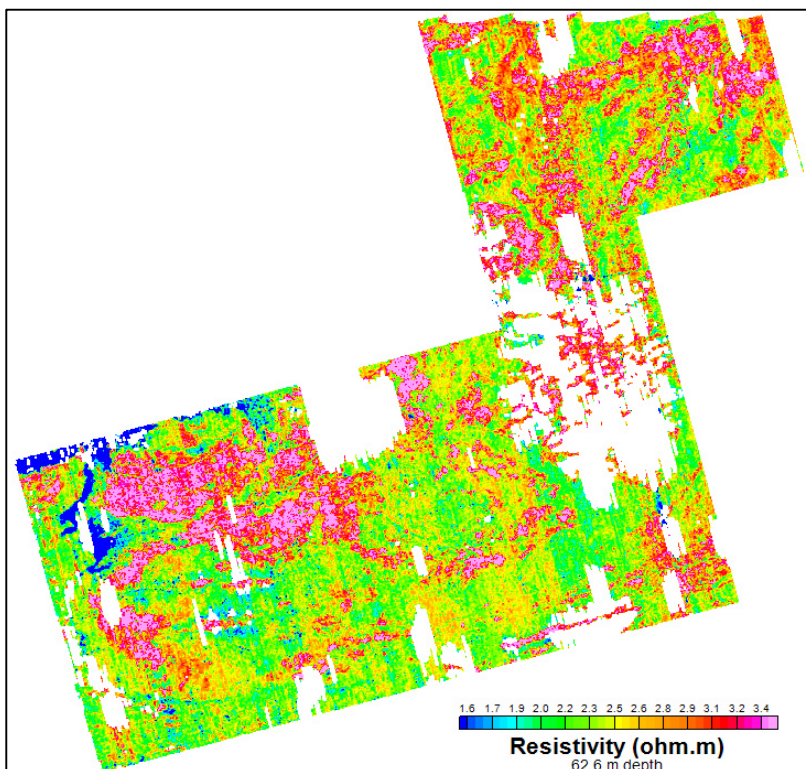


Figure 5.9: A5 Block EM inversion – grid maps of resistivity for 29.9 m depth layer. (Top) Final cleaned dataset. (Bottom) Final cleaned dataset after microlevelling. Models are blanked where solutions fall outside the threshold limits of the three QC criteria applied: NsensD29.9, QCpdiffD29.9 and P3resid. Minimum curvature gridding is used, with 50 x 50 m grid mesh.



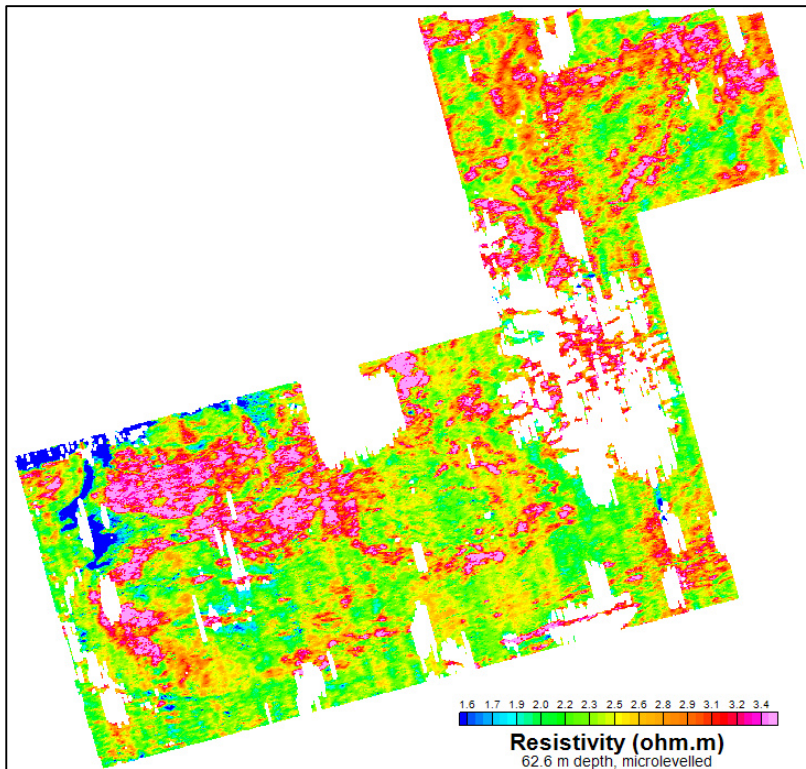


Figure 5.10: A5 Block EM inversion – grid maps of resistivity for 62.6 m depth layer. (Top) Final cleaned dataset. (Bottom) Final cleaned dataset after microlevelling. Models are blanked where solutions fall outside the threshold limits of the three QC criteria applied: NsensD62.6, QCpdiffD62.6 and P3resid. Minimum curvature gridding is used, with 50 x 50 m grid mesh.

Model Data Released

Bulk examination of inversion sensitivity profiles across the A5 Block indicate a general, marked reduction in model sensitivities below depths of around 50 – 60 m for model resistivities in the broad range 50 – 1,000 Ω .m (e.g., roughly $\pm 1\sigma$ or 68% of the data for layer D62.6). Below around 60 m depth, the resistivity models show little variation with increasing depth, suggesting they are largely weakly constrained extrapolations of well-constrained resistivity values modelled at shallower depth. Models for public release therefore do not include layers deeper than 62.6 m, providing a dataset with a reliable maximum depth of investigation.

EM inversion resistivity models, to a depth of 62.6 m, are released in a number of different data formats. The first dataset below constitutes the final and complete EM model dataset, with other datasets released being derivative products of this “master” dataset.



- i. **Ascii, flight-line and site ordered dataset.** Complete, full-resolution dataset with nominal 6 m spacing between model sites. Resistivity data for twenty depth-layers, from 1.0 m to 62.6 m depth, are provided as separate channels (columns) in the dataset. The data are suitable for manipulation to produce either section or map views of the models. Surface topography (DEM) with respect to sea-level is included for each site, allowing models to be plotted beneath a topographic reference in section view.

File name: [A5_EM_INV_MODELS_OHMM.XYZ].

File format: *Geosoft* [.XYZ]. Suitable for import into to any software with ascii import capability.

Dataset description: Appendix 1.

- ii. **Resistivity grids on 50 x 50 m mesh.** Provided separately for twenty depth-layers, from 1.0 m to 62.6 m depth.

File formats: *Geosoft* grid [.GRD] and georeferenced tiff [.TIF]

Dataset description: Appendix 2.



6. Conclusions

Using the A5 Block as a first test case, a new workflow for 1-D inversion modelling of Tellus EM data has been established, built around the capacities provide by a new, *Python* based software toolbox, *aempy*. *Python* scripting allowed a number of components of the inversion workflow to be customised and automated, including inversion parameter testing, bulk inversion of multiple flight-lines and customised output of both resistivity models and model quality assessment parameters. The latter have proven essential in the objective and automated rejection of poor model solutions, arising predominantly in high-fly areas where geological signal strength is significantly attenuated, but also in areas where data quality is negatively impacted by cultural noise.

1-D resistivity models were computed for a total of 3,725,100 sites on 525 flight-lines using Tikhonov-type, regularised inversion, implemented in *aempy*. The inversions produced a good overall quality of fit with respect to the observed EM responses: a mean RMS error of 1.516 and mean absolute value misfit residual of 67 ppm, calculated for sites with flight-clearance < 120 m (3,177,858 sites, or 85.3% of the A5 total). The RMS error reported is normalised by the data errors applied (60.0 ppm for all eight EM data components), with an RMS error value of 1.0 indicating a model fit to within the data error. Misfit residual is defined as the predicted model response minus the observed response, separately for each component (from which the mean value is derived).

Assessment of the model misfit residuals also provides insights into several broader characteristics of the A5 Block EM dataset, with potential to support ongoing EM data processing work of Tellus contractor SGL. The largest average inversion misfits are associated with the 12 and 25 kHz in-phase components and the 12 kHz quadrature component, indicating a general difficulty in matching the “baselines” of these observed data in the inversion models. Considering the A5 data subset with flight clearance < 120 m, predicted in-phase responses for 12 and 25 kHz are on average ~50 ppm lower and ~113 ppm higher respectively than the observed responses. Predicted quadrature responses for 12 kHz are on average ~70 ppm lower. Further, the testing of different errors assigned to the EM data components revealed a marked trade-off in the closeness of fit between the 12 and 25 kHz data components (an improved fit to one frequency



resulted in a poorer fit to the other) and a difficulty in matching the baselines of both frequencies simultaneously. Possible imbalances between the baselines of the observed 12 and 25 kHz data is an issue, therefore, that merits further examination together with contractor SGL.

Model cleaning – rejection of poor model solutions arising in high-fly and high-cultural-noise survey areas – was carried out in *Geosoft Oasis Montaj* software, using scripts that automated the sequential steps in the cleaning process. Three different QC parameters were found to be both necessary and adequate for rejection of poor solutions: (i) *Nsens*, the normalised model sensitivity, applied only where flight-clearance > 90 m (ii) *QCpdiff*, the percentage difference between the forward and reverse line direction inversion models, with respect to the average model, and (iii) *P3resid*, the 3 kHz in-phase misfit residual. Rejection threshold values for the three QC parameters were determined empirically by closely examining the relationship between the model solutions (good and bad) and the QC parameters, at all depths in the model and on multiple flight-lines across the survey area. The initial 35 layers of the inversion were truncated to 20 layers, from surface to 62.6 m depth, taking into account the marked reduction in model sensitivity below around 50 – 60 m depth observed broadly across the survey area. The final model dataset, therefore, retains only model solutions that pass the screening of the QC criteria and fall within a depth range where the EM data provide a strong model constraint.

The ~60 m depth of investigation and the lateral and vertical resolution characteristics of the model dataset make it well suited to a range of different possible applications where knowledge of shallow subsurface geology is required. Examples of potential uses include, but are not limited to: bedrock mapping (beneath the 3 – 7.5 m thick overburden typically encountered across much of the A5 Block) and high-resolution mapping of shallow geological strata; identification and mapping of shallow sand and gravel bodies; mapping of quaternary sedimentary deposits; soil mapping; thickness mapping of peat bogs; and shallow aquifer mapping.



7. References

Golub, G. and van Loan, C.F., 1996. *Matrix Computations*. The Johns Hopkins University Press, Baltimore, Maryland, 3rd Edition, pp. 694.

Kiyan, D. and Rath, V., 2017. Inverse Methods for Airborne Electromagnetic Data from the Tellus Surveys: The aempy Toolbox. Unpublished Report and User Manual, Dublin Institute for Advanced Studies, Ireland, March 21, 2017.

Kiyan, D., Rath, V., Delhaye, R., Ture, M.D. and Hodgson J., 2017. Imaging the Earth's Near Surface Using the Tellus Airborne Electromagnetic Data. Unpublished Presentation, Tellus Stakeholder Day, Geological Survey Ireland, Dublin, November 6, 2017.

Kiyan, D., Rath, V., Muller, M.R., Ture, M.D. and Hodgson, J., in review. Improved 1-D Inversion and Interpretation of Frequency-Domain Airborne Electromagnetic Data using aempy Toolbox. Manuscript submitted and in review.

Lanczos, C., 1961. *Linear Differential Operators*. D. Van Nostrand Co. Ltd, London, pp. 576.

Minsley, B.J., Smith, B.D., Hammack, R., Sams, J.I. and G. Veloski, G., 2012. Calibration and filtering strategies for frequency domain electromagnetic data. *Journal of Applied Geophysics*, **80**, 56–66.

Reninger, P.-A., Martelet, G., Deparis, J., Perrin, J. and Y. Chen, Y., 2011. Singular value decomposition as a denoising tool for airborne time domain electromagnetic data. *Journal of Applied Geophysics*, **75(2)**, 264 – 276.

Sengpiel, K. P., 1988. Approximate Inversion of Airborne EM Data from a Multilayered Ground. *Geophysical Prospecting*, **36**, 446-459.

Sengpiel, K.-P. and Siemon, B., 1998. Examples of 1D Inversion of Multifrequency AEM Data from 3D Resistivity Distributions. *Exploration Geophysics*, **29**, 133-141.

SGL, 2019. *Fixed-Wing High-Resolution Aeromagnetic, Gamma-ray Spectrometric and Frequency-Domain Electromagnetic Survey, Tellus A7 Block, Republic of Ireland, 2019*. Unpublished Technical Report, Sander Geophysics Limited, Canada, August, 2019.



Appendix 1: A5_EM_INV_MODELS_OHMM_ReadMe.txt

=====
This readme file relates to data from file: A5_EM_INV_MODELS_OHMM.XYZ (for lines L5001_L5525)

1-D inversion model data derived from airborne electromagnetic (EM) geophysical data collected during 2018_2019 by Geological Survey Ireland, Tellus Project.

Notepad text editor is recommended to read the data file correctly.

Data type: The data are 1-D EM inversion models for the A5 survey block.

Data modelling: Inversion models computed using aempy software, Tikhonov-type 1-D layered model inversion.

Model solutions nulled where failing QC criteria. Microlevelled.

Date of collection: EM data collected between 21/08/2018 and 29/03/2019.

Geographical extent: The A5 Survey block covers the majority of County Limerick and Tipperary, Ireland.

Contractor: Sander Geophysics Ltd

Client: Geological Survey Ireland (GSI)

Date of data release: 28 February 2020

For data queries please contact: tellus@gsi.ie

The data file contains the channels (columns) described below.

File header lines at start of file specified with "/" or "/" characters (without inverted commas)

Dataset is flight-line ordered, with a line separator "LINE line_number" at the start of each flight-line in the file (without inverted commas, and where line_number is numeric, e.g., 5260.0).

=====

File Name: A5_EM_INV_MODELS_OHMM.XYZ

Name	Units	Description
LINE	-	Line Number
ITM_X	m	X coordinate, IRENET95 ITM
ITM_Y	m	Y coordinate, IRENET95 ITM
DEM	m	Digital Elevation Model with respect to Mean Sea Level, from Laser Altimeter and GPS Z data
ALT	m	Flight clearance above Terrain, from Laser Altimeter
ResD1_0_ohmm	ohm.m	Model resistivity at 1.0 m depth, data nulled where failing QC criteria
ResD3_1_ohmm	ohm.m	Model resistivity at 3.1 m depth, data nulled where failing QC criteria
ResD5_2_ohmm	ohm.m	Model resistivity at 5.2 m depth, data nulled where failing QC criteria
ResD7_5_ohmm	ohm.m	Model resistivity at 7.5 m depth, data nulled where failing QC criteria
ResD9_8_ohmm	ohm.m	Model resistivity at 9.8 m depth, data nulled where failing QC criteria
ResD12_3_ohmm	ohm.m	Model resistivity at 12.3 m depth, data nulled where failing QC criteria
ResD14_9_ohmm	ohm.m	Model resistivity at 14.9 m depth, data nulled where failing QC criteria
ResD17_6_ohmm	ohm.m	Model resistivity at 17.6 m depth, data nulled where failing QC criteria
ResD20_5_ohmm	ohm.m	Model resistivity at 20.5 m depth, data nulled where failing QC criteria
ResD23_5_ohmm	ohm.m	Model resistivity at 23.5 m depth, data nulled where failing QC criteria
ResD26_6_ohmm	ohm.m	Model resistivity at 26.6 m depth, data nulled where failing QC criteria
ResD29_9_ohmm	ohm.m	Model resistivity at 29.9 m depth, data nulled where failing QC criteria
ResD33_3_ohmm	ohm.m	Model resistivity at 33.3 m depth, data nulled where failing QC criteria
ResD36_9_ohmm	ohm.m	Model resistivity at 36.9 m depth, data nulled where failing QC criteria
ResD40_7_ohmm	ohm.m	Model resistivity at 40.7 m depth, data nulled where failing QC criteria
ResD44_7_ohmm	ohm.m	Model resistivity at 44.7 m depth, data nulled where failing QC criteria
ResD48_9_ohmm	ohm.m	Model resistivity at 48.9 m depth, data nulled where failing QC criteria
ResD53_2_ohmm	ohm.m	Model resistivity at 53.2 m depth, data nulled where failing QC criteria
ResD57_8_ohmm	ohm.m	Model resistivity at 57.8 m depth, data nulled where failing QC criteria
ResD62_6_ohmm	ohm.m	Model resistivity at 62.6 m depth, data nulled where failing QC criteria

=====

Appendix 2: A5_EM_INV_MODELS_OHMM_GRIDS_ReadMe.txt

=====
This readme file describes raster grids provided in the file: [A5_EM_INV_MODELS_OHMM_GRIDS.zip]

Raster grids of 1-D inversion model data derived from airborne electromagnetic (EM) geophysical data collected during 2018_2019 by Geological Survey Ireland, Tellus Project.

Data type: Data are raster grids of 1-D EM inversion models for the A5 survey block.

Data modelling: Inversion models computed using aempy software, Tikhonov-type 1-D layered model inversion. Model solutions nulled where failing QC criteria. Microlevelled. Gridded at 50 m x 50 m mesh using Inverse Distance Weighted algorithm.

Date of collection: EM data collected between 21/08/2018 and 29/03/2019.

Geographical extent: The A5 Survey block covers the majority of County Limerick and Tipperary, Ireland.

Contractor: Sander Geophysics Ltd

Client: Geological Survey Ireland (GSI)

Date of data release: 28 February 2020

Two different georeferenced grid formats are provided for the Tellus geophysical data grids:

.grd files are Geosoft grid files and can be opened in: GIS software including Geosoft, ArcGIS (only with Geosoft ArcGIS plugin) and MAPINFO.

.tif files are georeferenced coloured raster files (GeoTiff files).

Instructions on how to display the grids with the correct colour ramp in ArcGIS and QGIS are in the [ArcGIS_Colour_Ramp_gxf_InstructionsReadMe.pdf] and [QGIS_Colour_Ramp_gxf_InstructionsReadMe.pdf] files included in this .zip.

Images are intended to be viewed with in the Geosoft Clra 32 colour ramp. Included in this .zip file are an ArcGIS style file [Geosoft.Style] and an QGIS XML Colour ramp [Geosoft_Clra_32_qgis.XML] that contain Geosoft Clra 32 colour ramps.

For data queries please contact: tellus@gsi.ie

The data contain the grids described below:

Name	Unit	DESCRIPTION
ResD1_0_ohmm_IDW	ohm.m	Model resistivity grid at 1.0 m depth, data nulled where failing QC criteria
ResD3_1_ohmm_IDW	ohm.m	Model resistivity grid at 3.1 m depth, data nulled where failing QC criteria
ResD5_2_ohmm_IDW	ohm.m	Model resistivity grid at 5.2 m depth, data nulled where failing QC criteria
ResD7_5_ohmm_IDW	ohm.m	Model resistivity grid at 7.5 m depth, data nulled where failing QC criteria
ResD9_8_ohmm_IDW	ohm.m	Model resistivity grid at 9.8 m depth, data nulled where failing QC criteria
ResD12_3_ohmm_IDW	ohm.m	Model resistivity grid at 12.3 m depth, data nulled where failing QC criteria
ResD14_9_ohmm_IDW	ohm.m	Model resistivity grid at 14.9 m depth, data nulled where failing QC criteria
ResD17_6_ohmm_IDW	ohm.m	Model resistivity grid at 17.6 m depth, data nulled where failing QC criteria
ResD20_5_ohmm_IDW	ohm.m	Model resistivity grid at 20.5 m depth, data nulled where failing QC criteria
ResD23_5_ohmm_IDW	ohm.m	Model resistivity grid at 23.5 m depth, data nulled where failing QC criteria
ResD26_6_ohmm_IDW	ohm.m	Model resistivity grid at 26.6 m depth, data nulled where failing QC criteria
ResD29_9_ohmm_IDW	ohm.m	Model resistivity grid at 29.9 m depth, data nulled where failing QC criteria
ResD33_3_ohmm_IDW	ohm.m	Model resistivity grid at 33.3 m depth, data nulled where failing QC criteria
ResD36_9_ohmm_IDW	ohm.m	Model resistivity grid at 36.9 m depth, data nulled where failing QC criteria
ResD40_7_ohmm_IDW	ohm.m	Model resistivity grid at 40.7 m depth, data nulled where failing QC criteria
ResD44_7_ohmm_IDW	ohm.m	Model resistivity grid at 44.7 m depth, data nulled where failing QC criteria
ResD48_9_ohmm_IDW	ohm.m	Model resistivity grid at 48.9 m depth, data nulled where failing QC criteria
ResD53_2_ohmm_IDW	ohm.m	Model resistivity grid at 53.2 m depth, data nulled where failing QC criteria
ResD57_8_ohmm_IDW	ohm.m	Model resistivity grid at 57.8 m depth, data nulled where failing QC criteria
ResD62_6_ohmm_IDW	ohm.m	Model resistivity grid at 62.6 m depth, data nulled where failing QC criteria
